Chemical Science

ROYAL SOCIETY OF CHEMISTRY

PERSPECTIVE

View Article Online
View Journal | View Issue

Cite this: *Chem. Sci.*, 2025, **16**, 10083

All publication charges for this article have been paid for by the Royal Society of Chemistry

Received 5th February 2025
Accepted 15th May 2025

DOI: 10.1039/d5sc00918a

rsc.li/chemical-science

Precise detection of G-quadruplexs in living systems: principles, applications, and perspectives

Huanhuan Li, Zelong Jin, Shuxin Gao, Shi Kuang,* Chunyang Lei and Zhou Nie *

G-quadruplexes (G4s) are non-canonical nucleic acid secondary structures that play a crucial role in regulating essential cellular processes such as replication, transcription, and translation. The formation of G4s is dynamically controlled by the physiological state of the cell. Accurate detection of G4 structures in live cells, as well as studies of their dynamic changes and the kinetics of specific G4s, are essential for understanding their biological roles, exploring potential links between aberrant G4 expression and disease, and developing G4-targeted diagnostic and therapeutic strategies. This perspective briefly overviews G4 formation mechanisms and their known biological functions. We then summarize the leading techniques and methodologies available for G4 detection, discussing the principles and applications of each approach. In addition, we outline strategies for the global detection of intracellular G4s, methods for conformational recognition, and approaches for targeting specific sequences. Finally, we discuss the technical limitations and challenges currently facing the field of G4 detection and offer perspectives on potential future directions. We hope this review will inspire further research into the biological functions of G4s and their applications in disease diagnosis and therapy.

Introduction

G-quadruplexes (G4s) are secondary nucleic acid structures in guanine-rich sequences.[1] They play critical roles in fundamental biological processes, including replication,[2] transcription,[3] telomere homeostasis,[4–6] translation,[7] RNA metabolism,[8] and epigenetic reprogramming.[9,10] Structurally, G4s are composed of stacked guanine tetrads (G-tetrads), which are planar units stabilized by Hoogsteen hydrogen bonds. π–π stacking interactions between G-tetrads and the coordination of monovalent cations such as K^+ or Na^+ further stabilize the structure.[11–14] In canonical intramolecular G4s, a single nucleic acid strand contains at least four guanine-rich repeats (GGG), separated by loop regions typically comprising one to seven nucleotides.[15] By contrast, intermolecular G4s are formed through guanine interactions across multiple nucleic acid strands, leading to bimolecular (two strands) or tetramolecular (four strands) assemblies. The structural diversity of G4s is remarkable and is influenced by various factors, such as strand polarity, loop orientation, folding topology, loop conformation, and capping structures.[16–18]

G4s are widely distributed across a diverse range of organisms, including animals (*e.g.*, humans, mice),[19–21] plants (*e.g.*, wheat, rice, and peas),[22–24] and pathogens.[25–28] High-throughput sequencing techniques such as G4-seq and RNA G4-seq have identified over 700 000 putative DNA G4s (dG4s) sequences and more than 3000 potential RNA G4s (rG4s) sequences in the human genome and transcriptome, respectively.[19,20,29] Besides, computational predictions suggest approximately 1 million potential G4 motifs exist in the wheat genome, with a density of 76–93 G4s per million base pairs. These structures are particularly enriched at transcription start sites (TSS), coding sequences (CDS), and promoter regions.[23] These studies have provided important reference maps for the potential formation of G4 structures under *in vitro* conditions. However, these methods do not account for the complex intracellular environment or the regulatory role of proteins in G4 formation. Developing efficient and robust detection tools is essential to understand whether these putative G4 sequences can form actual G4 structures in live cells and elucidate their role in regulating biological processes. Such tools should enable *in situ* detection of G4s in live cells and even in whole animals, facilitating the measurement of G4 formation, abundance, conformation, subcellular localization, and dynamic behaviour.

To date, various techniques have been employed to study G4s, including chemical mapping,[30–32] circular dichroism (CD) spectroscopy,[33–35] X-ray crystallography,[36–40] nuclear magnetic resonance (NMR) spectroscopy,[41–50] and fluorescence imaging.[19,51–58] Chemical mapping approaches, such as those using potassium permanganate, dimethyl sulfate (DMS), or 2′-acylation reagents, exploit differences in chemical reactivity between G4s and other nucleic acid structures. For example, DMS methylates G4s at significantly lower rates than single-stranded or double-stranded DNA due to the Hoogsteen

State Key Laboratory of Chemo and Biosensing, Hunan Provincial Key Laboratory of Biomacromolecular Chemical Biology, Hunan University, Changsha 410082, People's Republic of China. E-mail: niezhou.hnu@gmail.com; kuangshi@hnu.edu.cn

hydrogen bonds in G4s.[31] CD spectroscopy rapidly differentiates G4 topologies, while X-ray crystallography and NMR spectroscopy offer atomic-level structural insights. However, chemical mapping reagents are generally toxic to cells, and their readouts represent averaged structural states;[9] CD spectroscopy has limited resolution when studying interactions between G4s and G4-binding proteins or ligands; and X-ray crystallography requires crystallized samples, which may not accurately reflect the physiological state of G4s.[59] These limitations obstruct its capability to detect G4s in complex intracellular environments and make it unsuitable for detecting G4s in live cells.

In contrast, fluorescence-based techniques and NMR spectroscopy have emerged as powerful tools for studying G4s in live cells due to their non-invasive nature and suitability for analysing of complex systems.[41,43,51,58,60–65] Fluorescence-based methods, which monitor changes in fluorescence distribution, intensity, or the lifetime of the probes upon binding to G4s, have been widely used for imaging G4s abundance,[61] conformations,[51,54,66] sequence specificity,[56,57,67] and G4-related protein[68,69] in live cells and animals. Fluorescence techniques offer high resolution and sensitivity, making them key tools for investigating G4s functions. On the other hand, NMR techniques can directly probe the conformation of G4s at atomic resolution by analysing changes in NMR signals from specific atoms (*e.g.*, imino protons). Notably, introducing (such as ^{19}F, ^{13}C, ^{15}N) into specific positions helps simplify background interference,[43,49,70] providing clear and direct information for establishing cellular G4s "fingerprint" maps and studying their dynamic behaviors.[41]

Even though *in vitro* studies have demonstrated the regulatory roles of G4s in transcription, translation, genomic stability, and disease-associated gene expression, the dynamic nature of G4s is affected by multiple factors, including complex RNA-binding protein interactions, epigenetic modifications, chromatin accessibility, and transcriptional activity, which cannot be fully replicated *in vitro*.[71] These factors highlight the significance of detecting G4s *in situ* within live cells. Currently, NMR and fluorescence methods are widely used to investigate the structure, distribution, and biological functions of G4s in live cells. However, existing reviews primarily focus on G4 structures in specific genes,[72] imaging techniques for G4 detection,[73] and the interactions between G4s and ligands, and related methodologies.[59] To date, no reviews have focused on methods that reveal the dynamic structure and function of G4s under physiological conditions, which are essential for establishing links between G4s and disease diagnosis and treatment. Therefore, this review focuses on *in situ* imaging and detection techniques for studying G4s in living systems and explores their relationship with related diseases (Table 1).

We first introduce the structure of G4s and compare the differences in structure and chemical properties between dG4s and rG4s. Next, we provide an overview of the mechanisms underlying G4 formation, their biological significance, and their associations with disease. We then discuss fluorescence-based and NMR techniques, emphasizing their principles, applications, and contributions to understanding G4 dynamics, folding, and sequence specificity in cellular contexts. Finally, we address the limitations of current detection methods and propose future directions for G4 research, including developing novel detection strategies. We hope this review serves as a valuable resource to advance our understanding of G4 biology and its potential applications in disease diagnosis and therapeutic development.

Structural diversity of G4s

G4s can adopt various topological structures, such as parallel, antiparallel, and hybrid conformations, depending on the orientation of the G4 strands (Fig. 1a).[74] The final confirmation of a G4 depends on the glycosidic bond conformation (*anti* or *syn*) between guanine and pentose sugar (Fig. 1b). In addition to variations in strand orientation and glycosidic bond conformation, the type of loops (*e.g.*, propeller, diagonal, and lateral) and the width of the grooves (wide, medium, or narrow) also differ across various G4 topologies.[12,15,75,76]

While DNA and RNA can form G4s similarly, they exhibit some differences in structure and chemical properties.[77] First, dG4s can adopt parallel, antiparallel, or hybrid conformations, while rG4s predominantly form parallel structures due to the *anti*-conformation of glycosidic bonds in ribonucleosides. Second, rG4s exhibit superior thermal stability compared to dG4s, attributed to hydrogen bonding from the 2′-OH group in the ribose sugar and the networks of water-mediated contacts within the grooves of RNA.[78–82] Third, their ion preferences differ significantly, dG4s respond to Na^+ and K^+, whereas rG4s show strong K^+ selectivity.[83,84] Fourth, due to structural diversity and wider grooves of dG4s, which shows better ligand binding capacity varies substantially, while rG4s face steric constraints from the 2′-OH group.[85,86] Fifth, dG4s formation requires double-strand separation or chromatin remodeling in genomic DNA, while rG4s form dynamically in single-stranded transcripts and are readily modulated by RNA-binding proteins.[87,88] These fundamental differences underlie their distinct biological roles.

dG4s and rG4s exhibit significant differences in chemical properties. From a kinetic perspective, the folding of rG4s follows a monophasic process, while dG4s formation undergoes a biphasic transition involving conformational conversion from double-stranded DNA (dsDNA) to dG4s. Therefore, rG4s show significantly faster folding kinetics, achieving stable conformations in substantially shorter timeframes, which reduces the effective window for chemical modifications. dG4s exhibit higher flexibility in glycosidic bond conformations, facilitating interconversion between different topological arrangements. This results in greater solvent exposure of loop regions in dG4s, thereby increasing the accessibility of reactive sites to chemical probes. In addition, the structural stability of G-quadruplexes critically influences the efficiency of chemical labeling approaches. Conventional labeling techniques, such as dimethyl sulfate (DMS) methylation, primarily target the nucleophilic N7 atoms of guanines when the G4 structure is in a single-stranded state.[31] The presence of 2′-hydroxyl groups in rG4s confers more excellent structural stability compared to

Table 1 Advantages, limitations, and suitable applications of methods for studying G4s

Method	Advantage	Limitation	Suitable applications
Circular dichroism (CD)	It provides melting temperature curves and typology changes, which are useful for rapidly determining the structure of G4s *in vitro*	Low resolution when studying interactions between G4s and G4-binding proteins or ligands	Identifying the polarity of chains and quickly determining G4 structures *in vitro*
X-ray crystallography	It allows detailed atomic-level structural and spatial characterization, including ligand binding sites, through electron density maps. It is relatively inexpensive and straightforward	Requires crystallizable samples and a large amount of G4s. Provides only static, three-dimensional data and is limited to *in vitro* studies	Detailed structural and spatial characterization of G4s and interactions with ligands *in vitro*
Chemical mapping	Determines nucleic acid (DNA and RNA) secondary and tertiary structures at single-nucleotide resolution; penetrates cells and cellular compartments	Averaged readout of structural states. High cellular toxicity and experimental conditions may shift G4 formation, not reflecting the true cellular state	Mapping G4s within the genome and transcriptome *in vitro*
Nuclear magnetic resonance (NMR)	Provides atomic-resolution characterization of G4s. Enables direct identification of G4s typology in live cells	Requires the introduction of exogenous G4 sequences to enhance concentration and signal response. Time-consuming	Determining G4's three-dimensional structure in solution, identifying G4 typology, and tracking dynamic changes in live cells
Fluorescence imaging	Offers information on the distribution and dynamic changes of G4s in live cells	The dynamic equilibrium of G4 formation may be altered during the experiment, leading to inaccuracies in reflecting the true cellular state. It also depends on probe specificity and photobleaching	Imaging G4 abundance, conformation, and G4-related proteins in live cells and animals. Useful for investigating the dynamic formation of G4s in live cells

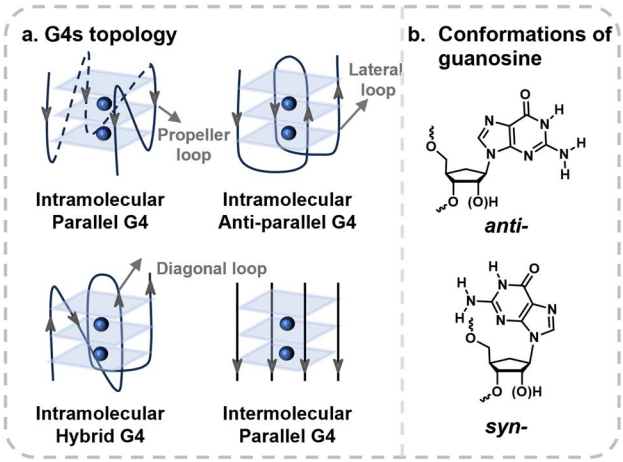

Fig. 1 (a) G-quadruplex topology, including intermolecular and intramolecular G4s. (b) *Anti*- and *syn*-conformations of guanosine in a G-quartet.

dG4s, which reduces the exposure of reactive sites during DMS methylation and consequently decreases the reaction kinetics.

Recent methodological developments in computational methods for G4s extend our understanding of G4s-related functions. The existing computational methods are mainly divided into three categories: regex-based, scoring-based, and machine learning-based methods.[89] Regex-based methods are developed based on the empirical regexes, such as Quadparser, which uses $G_{3-5}N_{1-7}G_{3-5}N_{1-7}G_{3-5}N_{1-7}G_{3-5}$ and has identified approximately 376 000 G4s in the human genome.[90] However, regex-based methods often ignore the nonstandard motif of non-canonical structures. Scoring-based algorithms often use more flexible regexes, which have less strict criteria and provide more possibilities to predict the sequence most likely to form non-canonical G4s. Representative scoring-based algorithm QGRS mapper uses $G_xN_{y1}G_xN_{y2}G_xN_{y3}G_x$ ($x \geq 2$) to search for motifs and utilizes G-scores to evaluate whether a candidate motif can form a stable G4 structure.[91]

Moreover, novel score-based approaches PQS finder grant greater parameter liberty and tolerate G-run defects, such as bulges and mismatches in the detection process. It can also identify and resolve overlapping PQS, as many G4 sequences overlap and compete for the common nucleotides to form the final structures.[92] New sequencing techniques were developed to map G4s *in vitro* and G4s *in vivo*. Machine and deep learning-based methods were proposed to predict such regions, comprising the G4(s) and flanking sequences. For instance, Quadron, a machine learning approach, was proposed to predict G4s based on sequence features (such as *k*-mer occurrences) from a region of more than 100 bases and trained using *in vitro* G4 regions with G4-seq.[93] Lately, several machine learning based-methods using convolutional neural network (CNN) were developed, such as PENGUINN, G4detector, and DeepG4, which were used to predict nuclear G4s, genome-wide G4s, and cell-type specific active G4s region separately.[94–96] PENGUINN can measure the potential of a sequence with a length from 20 to 200 nt to form G4.[94] It surpasses state-of-the-art methods in simulating high-background testing sets with significant genomic variation. The model supports the

nematode *Caenorhabditis elegans* and the plant *Arabidopsis thaliana*, but its performance in these species is lower than that expected by humans or mice.[97] G4detector can predict the whole genome G4s with high accuracy and can apply these measurement results from human-trained data to various non-human species.[95,97] DeepG4 was designed to assess the ability of G4 sequences to form *in vivo*.[96] It focuses on predicting specific motifs in the active G4 region rather than G4 sequences with flexible patterns. Using human data as a training set, G4 detection of DeepG4 on non-mammalian genomes appears to be less accurate.[97] In addition, a machine learning-based method was developed for rG4s. rG4-seeker uses customized noise models to predict non-canonical G-quadruplexes (rG4) from rG4-sequencing (rG4-seq) data. It effectively reduces local sampling errors and background noise in rG4 sequences, allowing it to identify rG4 candidates with a high level of confidence.[98] The rG4-seeker shows improved sensitivity in discriminating against false-positive samples compared to previous methods.[97]

Biological function of G4s

Putative G4 sequences are widespread throughout the genome, but not all can fold into G4 structures. Their folding dynamics are regulated by cell type and physiological conditions.[99] Several factors can promote G4s formation, such as negative torsional stress induced by DNA or RNA polymerases at the replication fork and molecular crowding effects.[100,101] Specific G4s-binding proteins or partner proteins regulate G4s formation and stability, including nucleolin and RNA-binding protein RBM4.[102,103] The formation of G4s is thought to interfere with essential nucleic acid processes, such as replication, transcription, and translation.[9,104,105] For example, in the promoter region of the *MYC* oncogene, G4-stabilizing ligands, like TMPyP4, effectively suppress *MYC* protein expression, downregulating the activity of this oncogene.[106] Meanwhile, cellular mechanisms exist to unwind G4s structures, primarily mediated by helicases, including members of the RecQ-like, DEAD-box, and DEAH-box helicase families.[9,107,108] Furthermore, certain proteins that bind unfolded putative G4 sequences, such as cellular nucleic acid-binding protein (CNBP) and G-rich sequence factor 1,[109,110] as well as single-stranded DNA-binding proteins like protection of telomeres 1 (POT1) and replication protein A (RPA), regulate G4 function by stabilizing their unfolded states.[111]

G4s are crucial for maintaining genome stability and integrity. G4 structures can obstruct replication fork progression, leading to fork collapse and subsequent double-strand breaks, contributing to genomic instability (Fig. 2a).[112] Studies have shown that putative G4 sequences are significantly associated with DNA breakpoints in cancer tissues and mutation hotspots.[5,106,113–116] It is also reported that G4-stabilizing ligands, such as pyridostatin (PDS), can induce double-strand breaks at replication forks.[117] Moreover, computational analyses have shown that transcription factors are highly enriched in certain promoter G4 motifs.[118] Experimental evidence and structural basis have confirmed that nucleolin and NM23-H2 can stabilize and unwind G4s in the *MYC* promoter, respectively, and are likely to regulate *MYC* transcription.[102,119,120] G4s present on the template strand during transcriptional elongation hinder the progression of RNA polymerase, thus inhibiting transcription (Fig. 2b).[114,121]

Telomeres are the protective nucleoprotein structures located at the ends of chromosomes, which prevent abnormal DNA repair at the chromosome termini by binding to telomere-specific binding protein complexes and forming higher-order DNA structures.[122] Evidence suggests that in mammalian cells, the 3′ single-stranded G-rich overhang of the telomere can invade the upstream double-stranded telomeric DNA, forming a lasso-like t-loop in which G4 structures are formed.[6,123] When the telomere loop is disrupted, G4s act as a critical protective structure (Fig. 2c).[124] G4s and G4-stabilizing ligands can alter the binding of telomere-associated G4-interacting proteins, resulting in changes in telomere replication rates and/or the formation of fragile telomeres or telomere loss.[125] Telomerase, a non-coding RNA reverse transcriptase complex responsible for extending the chromosome ends of cancer cells, stem cells, and germline cells, can be regulated by G4 formation.[126] G4s modulate telomerase binding to telomeres, thereby preventing telomere shortening and genomic instability.[127–129] This regulation has inspired the development of various G4-targeting chemotherapeutic agents.[130,131]

rG4s have also attracted wide attention (Fig. 2d).[8] The density, thermodynamic stability, and positioning of G4s relative to the 5′ cap have been shown to affect translation in distinct ways.[132,133] Several reports confirm that G4 structures in the 5′ untranslated region (UTR) of mRNAs impede the scanning of the 5′-UTR and downregulate the translation efficiency of downstream proteins, such as in *KARS* mRNA and *BCL2* mRNA.[115,116] Beyond their direct effects on translation efficiency, G4s in the UTR are involved in stress granule formation and mRNA localization through interactions with G4-binding proteins (Fig. 2e).[134,135] In contrast, G4s are less common in the coding regions of mRNAs but still hinder mRNA entry into the ribosome and its binding to tRNA, induced translation stalling (Fig. 2d).[136,137] Moreover, G4s on mRNA worked as a positioning element for splicing and have been implicated in alternative splicing regulation (Fig. 2d). For example, rG4s facilitate the recruitment of splicing-related RNA-binding proteins, such as heterogeneous nuclear ribonucleoproteins (hnRNP H and hnRNP F), thereby influencing RNA splicing processes.[123,138]

Research has also established links between G4s and diseases.[25,26,134,139–141] For example, nucleotide repeat expansions are implicated in neurodegenerative diseases, including Huntington's disease (HD), fragile X syndrome, amyotrophic lateral sclerosis (ALS), and frontotemporal dementia (FTD).[139,142–144] Repeated GGGGCC motifs in the *C9ORF72* gene adopt G4 structures, sequestering splicing factors such as hnRNP H, leading to splicing dysregulation-a critical factor in ALS and FTD pathogenesis.[134] Similarly, G4s formed by AAGGG repeats in the *RFC1* gene impede DNA replication, and their presence in mRNA affects protein binding, splicing, and translation,

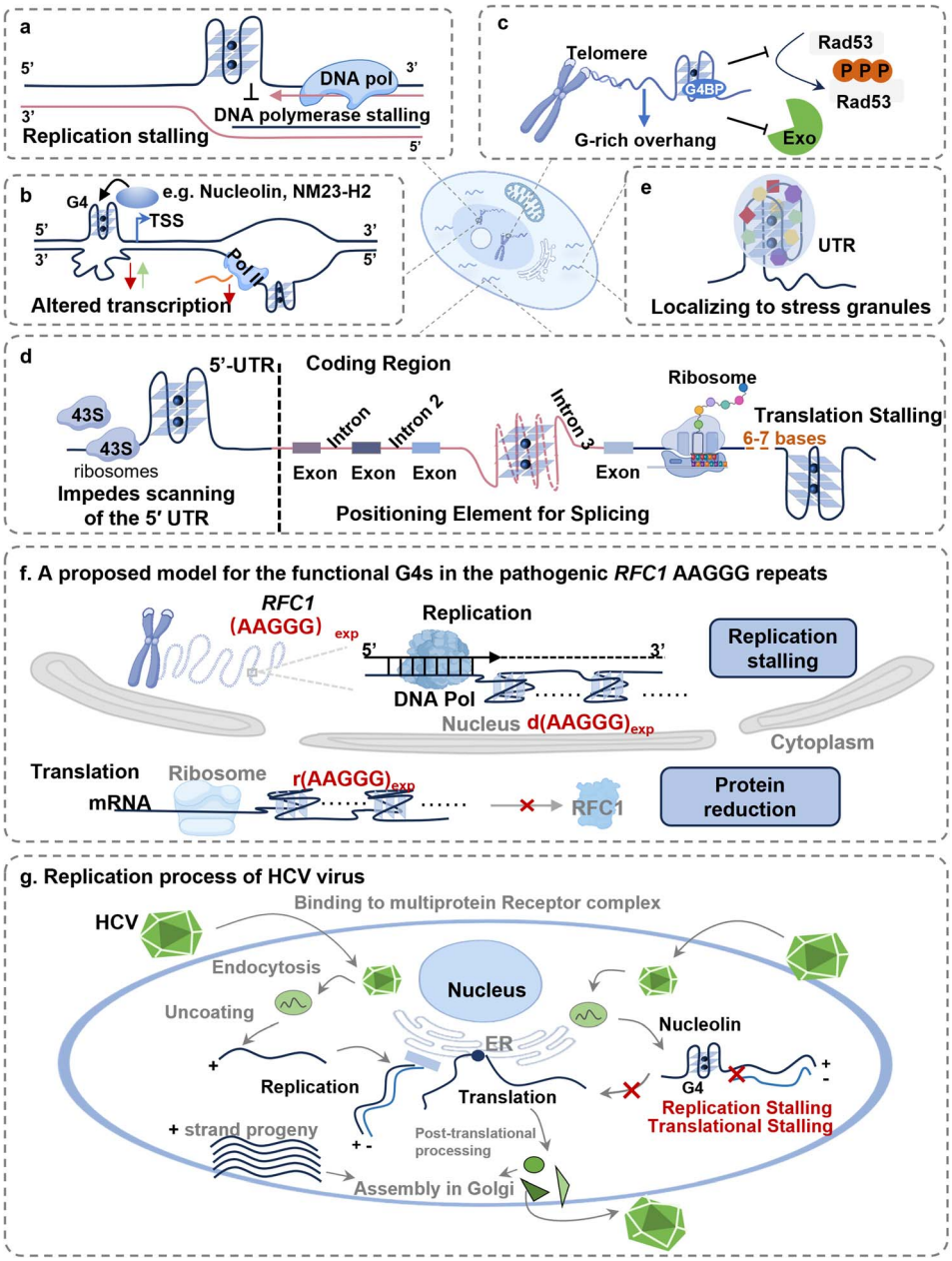

Fig. 2 Biological functions of G4s. (a) G4s impede DNA replication by stalling the replication fork. (b) dG4s located upstream of the transcription start site can either bind to or displace transcription factors, leading to alterations in transcription. During transcription elongation, G4 formation on the template strand can obstruct the progression of RNA polymerase II. (c) At uncapped telomeres, G4s DNA may interact with G-quadruplex binding proteins (G4BPs) to inhibit exonucleolytic degradation and prevent Rad53 checkpoint activation caused by the loss of Cdc13 function. This mechanism helps maintain telomere length and prevents telomere degeneration. (d) rG4 formation impedes the scanning of the 5′ untranslated region (UTR) by 43S ribosomes, which can shift the translation initiation site. In the coding region, recognition of rG4s by spliceosome-associated RNA-binding proteins influences the splicing of adjacent introns. Additionally, G4 formation in the coding region hinders mRNA entry into the ribosome and its binding to tRNA, thereby downregulating translation efficiency. (e) In the UTR, rG4s may also play a role in forming stress granules and participate in RNA location. (f) A proposed model for the functional consequences of G4s formation in the pathogenic *RFC1* AAGGG repeats. The expanded AAGGG repeats form dG4s that impede polymerase processivity and cause replication stalling, as well as rG4 structures that impair translation and reduce protein production. (g) Replication process of the HCV. G4-binding ligands and nucleolin stabilize the G4s in the core region of the HCV, leading to replication/translation stalling, which inhibits HCV proliferation.

ultimately causing cerebellar ataxia, neuropathy, and vestibular areflexia syndrome (Fig. 2f).[145]

G4s are also prevalent in viral genomes, including those of human immunodeficiency virus (HIV),[25] hepatitis C virus (HCV),[26,51] Zika virus,[27] Ebola virus,[28] and SARS-CoV-2.[146] Detecting and stabilizing viral G4s can inhibit viral genome replication and translation, providing a promising therapeutic strategy.[147] For instance, in HCV, G4 formation in the conserved

core region leads to premature RNA replication termination and suppression of core protein translation (Fig. 2g).[26] Similarly, in SARS-CoV-2, the RG-1 sequence in the coding region of the nucleocapsid phosphoprotein forms G4 structures in live cells.[146] Stabilizing these G4s with ligands has been shown to downregulate viral protein expression, highlighting G4s as potential antiviral targets.

Principles of G4s detection in cells

Detecting G4s in cells primarily relies on fluorescence-based methods and NMR techniques. Immunofluorescence and small-molecule fluorescence probes are the most commonly used fluorescence methods.[51,53,60,66,148–153] Immunofluorescence is considered one of the gold standards for detecting G4s within cells.[60,148] It relies on the use of specific antibodies, such as BG4, which bind to G4s through protein-nucleic acid integration. The binding is then detected using fluorescently labelled secondary or tertiary antibodies, enabling the visualization and quantification of G4s (Fig. 3a). The BG4 antibody, selected through phage display technology from a library containing 2.3×10^{10} different single-chain antibody clones, demonstrates high specificity and affinity for G4s. However, immunofluorescence is unsuitable for live-cell imaging since antibodies cannot cross the cell membrane. This limitation has driven the development of small-molecule fluorescence probes for G4 detection. To address these considerations, a camelid heavy-chain-only derived nanobody named SG4 that was selected against the human *MYC* dG4 structure was developed. It deployed SG4 *in situ* by expression in human cells for detecting and mapping G4s in the chromatin of human cancer cell lines.

Many small-molecule G4 fluorescence probes have recently been developed (Fig. 3b).[51,54,57,58,61,66,154] These G4-specific molecules typically contain multiple aromatic rings and exhibit negligible fluorescence in solution due to processes such as twisted intramolecular charge transfer (TICT), photo-induced electron transfer (PeT) or aggregation-caused quenching (ACQ).[155–158] Upon binding to G4s *via* π–π stacking interactions, these processes are suppressed, leading to fluorescence recovery and the creation of "turn-on" fluorescence probes.

TICT is an intramolecular charge transfer process in molecules where a rotatable single bond connects the donor and acceptor components (Fig. 3e).[157] Upon photoexcitation, electrons in the molecule are transferred from the donor to the acceptor, causing the donor and acceptor planes to rotate and resulting in a twisted molecular conformation. This twisted

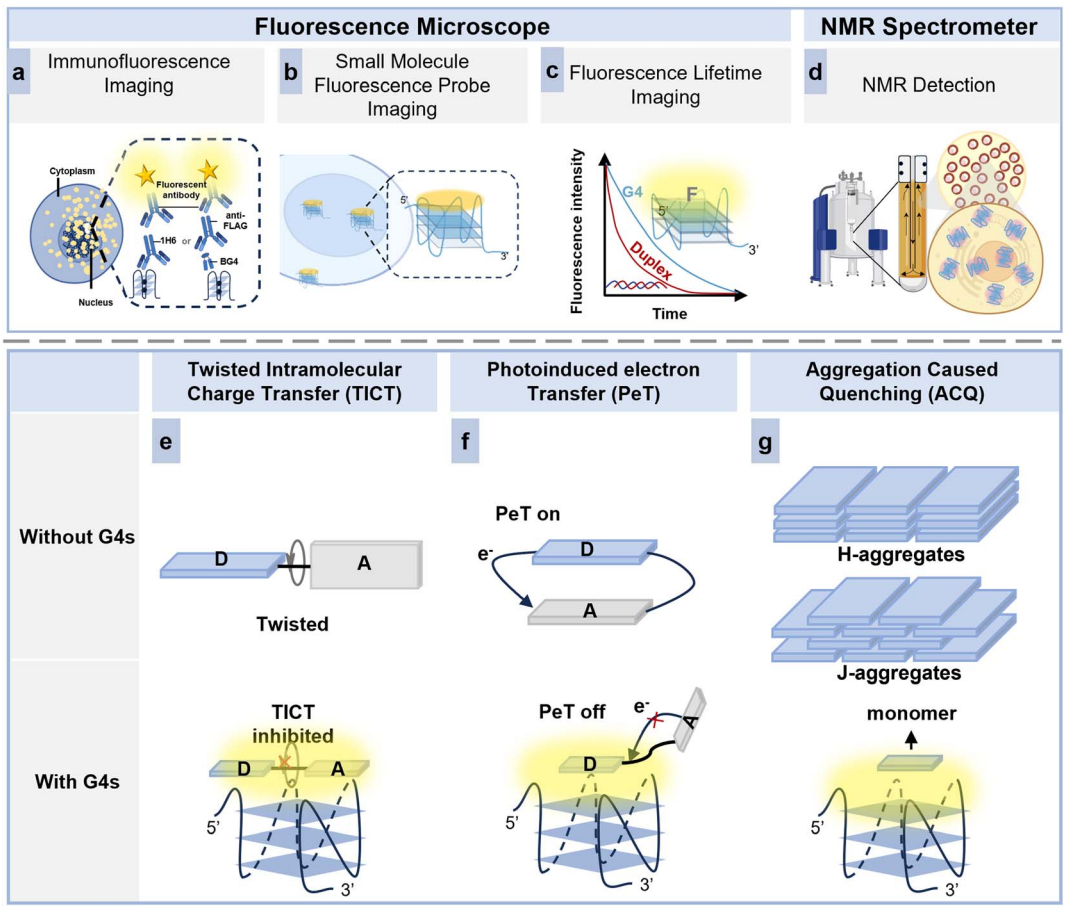

Fig. 3 Tools for detecting G4 structures in cells using different techniques. (a) Immunofluorescence imaging. (b) Small molecule fluorescence probe imaging. (c) Fluorescence lifetime imaging. (d) NMR detection. (e and f) Principles of small molecule probes used for G4 detection. (e) Twisted intramolecular charge transfer (TICT), (f) photo-induced electron transfer (PeT), and (g) aggregation-caused quenching (ACQ).

structure facilitates the relaxation of the molecule to its ground state through non-radiative transitions or redshifted emission. Probes exhibiting this phenomenon include the HCV imaging probes ThT-NE and NIR-2.[51,159] When these probes are not bound to G4s, the energy within the molecule is dissipated non-radiatively during the twisting process, preventing fluorescence emission. However, when these probes bind to G4s *via* π–π stacking interactions, the TICT process is inhibited, and the energy is released *via* fluorescence, thus "turning on" the probe. Another class of "turn-on" fluorescence probes is based on the PeT process (Fig. 3f). These probes typically consist of a fluorophore, a short spacer, and a receptor (G4 ligand), where the fluorophore absorbs and emits fluorescence. In contrast, the receptor binds to the G4 of interest and acts as the quencher.[156,158] In the absence of G4s, the fluorophore and G4s ligands are nearby. Upon excitation, electron transfer occurs between the fluorophore and the G4 ligand, inhibiting the return of the excited-state electron to the fluorophore's ground state, resulting in fluorescence quenching. When the probe binds to G4s, the fluorophore and G4 ligand are separated, preventing the photo-physical interaction and restoring fluorescence. An example is the NaphthoTASQ probe, which exhibits fluorescence recovery upon binding to G4s.[61] TICT and PeT mechanisms rely on intramolecular charge transfer, and ACQ arises from enhanced intermolecular π–π stacking interactions, leading to fluorescence quenching (Fig. 3g). In the presence of π–π stacking, molecules aggregate into J-aggregates or H-aggregates, causing the fluorophores to align closely.[155] This proximity significantly increases the rate of non-radiative transitions, such as external conversions and vibrational relaxation, which prevents excited-state electrons from returning to the ground state *via* radiative pathways, thus resulting in fluorescence quenching. Upon interaction with G4s, the probe molecules dissociate into monomers, restoring radiative transitions and enhancing fluorescence. For example, the red fluorescent dye CV2 self-assembles into nanoparticle aggregates that emit red excimer fluorescence in water. When bound specifically to G4s, the aggregates disassemble into monomeric dye molecules, leading to enhanced fluorescence.[66] In the fluorescence-based methods for detecting G4 structures in live cells mentioned above, the evaluation of target signal strength is typically achieved by measuring changes in the fluorescence emission intensity of probes.

However, this approach can be influenced by factors such as probe's local concentration, the excitation light's intensity, and environmental conditions, which may adversely affect the experimental results. To address these limitations, our team developed a ratiometric probe, NHCouI, by combining a green fluorescent protein (GFP) module with a coumarin 6H molecule.[154] This probe features dual-emission and self-calibration capabilities: a fixed green emission that serves as an environmental-insensitive reference for calibration and a red emission specifically activated by parallel G4 structures. The red-to-green fluorescence ratio is independent of the absolute fluorescence intensity, local probe concentration, environmental viscosity, and laser power, making it a more reliable indicator for live-cell G4 detection.

In addition to the rational design of fluorescence probes, fluorescence intensity-independent techniques, such as fluorescence lifetime imaging (FLIM), have also been introduced to overcome the aforementioned issues effectively (Fig. 3c).[58,160,161] Fluorescence lifetime refers to the average time a molecule remains in its excited state, which is affected by the molecular conformation of the fluorophore and its surrounding microenvironment. Measurement of fluorescence lifetime is independent of the probe and G4 concentration, as well as interactions between the probe and other nucleic acids.[162] This makes FLIM a highly specific and sensitive method for monitoring G4 structures, providing rich spatial and temporal information. The primary technique used in fluorescence lifetime imaging of G4s is Time-Correlated Single Photon Counting (TCSPC).[161] The basic principle of TCSPC involves using a pulsed laser as the excitation source and recording the time interval between the excitation pulse and the arrival of a single emitted photon. The TCSPC detector converts individual photons into electronic pulses and precisely measures their arrival time relative to the excitation pulse, offering excellent temporal resolution and accuracy in fluorescence lifetime measurements.

Compare to fluorescence-based techniques, NMR provides a higher-dimensional approach, enabling direct investigation of macromolecular structures and dynamics with high resolution in live cells (Fig. 3d).[63] NMR has been widely used to study G4 conformations, kinetics, and G4-ligand interactions.[41,43,47,163–165] In intracellular G4 studies using ^{1}H NMR, the chemical shifts of imino protons (which are associated with Hoogsteen base pairing, with chemical shifts typically ranging from 10–12.5 ppm), peak intensities, and line-width characteristics observed in solution are often used to infer the conformation of G4s in live cells and their interactions with ligands.[59,63] However, due to the complex intracellular environment, ^{1}H NMR-based detection methods are susceptible to interference from various cellular components. To obtain more detailed structural information, polarization transfer techniques, such as the nuclear Overhauser effect (NOE),[166] transferred-NOESY,[167] saturation transfer difference (STD),[168] and water-LOGSY,[50] can be employed. These methods provide finer insights but generally require longer sampling times and precise pulse control. An alternative strategy to mitigate background interference from the high abundance of hydrogen atoms in cells involves modifying the nucleic acid sequence with specific heteroatoms.[42] This approach enables the detailed structural information about G4 conformations in live cells.

Global detection of G4s in cells

G4s are higher-order nucleic acid structures that play a crucial role in cellular regulation and are involved in various biological processes.[60,99,169] The folding and unwinding of G4s are tightly regulated in both temporal and spatial dimensions at the cellular level. Live-cell and *in vivo* imaging of G4s is crucial for understanding the molecular mechanisms and regulatory pathways underlying their biological functions. Such imaging techniques offer valuable insights into the onset, progression,

and potential therapeutic strategies for diseases associated with G4 dysregulation. Fluorescence-based non-invasive imaging methods provide excellent spatiotemporal resolution, high sensitivity, and cost-effectiveness, making them indispensable tools for the study of G4s.[51,66,159,170–175] These techniques facilitate real-time, *in situ* imaging of G4s within live cells and even whole organisms, making them particularly valuable for investigating G4 regulation and their roles in cellular systems.

In 2013, highly specific dG4s antibodies, BG4 and 1H6, were used to confirm the formation of G4s in fixed mammalian cell DNA.[60,148] Development of small-molecule probes (Fig. 4a), such as NaphthoTASQ, provided effective means for studying the presence and dynamic changes of G4s in living cells.[61] This probe contains four guanine bases and a naphthalene ring. It is non-fluorescent in solution but can cross the cell membrane. Molecular dynamics simulations demonstrated that the guanine bases in NaphthoTASQ stack onto the G-plane of G4s through a bioinspired binding mode, inhibiting photo-induced electron transfer (PeT) between the guanine and naphthalene rings, thereby activating fluorescence. NaphthoTASQ enabled the first fluorescence-based *in situ* detection of G4s in live cells. Subsequently, a G4s ligand database (G4LDB), derived from the cyanine dye CyT, has been developed to distinguish rG4s from other RNA structures.[176,177] When CyT binds to rG4s, fluorescence increases by over 1000-fold, while it shows less than 25-fold enhancement with non-G4 RNA. Since then, numerous fluorescent probes, such as benzothiazole-, thiazole orange-, spiropyran-based, and coumarin-based compounds, have been explored for G4-specific fluorescence activation.[178] For example, the benzothiazole-based dual-color fluorescence probe $QCy(MeBT)_3$ was developed to selectively image double-stranded DNAs (dsDNAs) and G4s in cells, responding distinctly to AT-rich dsDNAs ($\lambda_{ex/em}$ = 470/660 nm) and dG4s/rG4s ($\lambda_{ex/em}$ = 570/700 nm).[152] IMT[179] and ThT-NA[55] probes have been used to track dG4 and rG4 dynamics during the cell cycle, respectively (Fig. 4b). Other notable examples include benzoselenazole derivatives m-Se3, which selectively stabilize dG4s in the c-*MYC* promoter, leading to selective inhibition of hepatoma cell proliferation.[180] Coumarin-related CQ with two-photon character and photo-switchable fluorescence capability can perform super-resolution imaging of mtDNA G4s in live HepG2 cells through STORM technology (Fig. 4c).[150] And spiropyran-based probes such as QIN, which enable the visualization of differential relative abundance of dG4s in the nuclei between normal and cancer cell lines (Fig. 4d),[181] as well as TANG, with low pK_a (4.3), which is stable to lysosomal acidity, transforms into a positively charged open-ring form and exhibits significant fluorescence enhancement while binds with intranuclear dG4s.[182]

Fluorescence-based molecular probes provide powerful tools for global studies of G4s in live cells. However, fluorescence intensity can be influenced by both the nucleic acid and local concentrations of small molecules, complicating interpretation. FLIM, a technique independent of fluorescence intensity, has emerged as a promising solution. FLIM differentiates G4s from other nucleic acid structures based on differences in fluorescence lifetimes when small-molecule ligands bind to G4s. The first FLIM probe reported, DAOTA-M2, a molecule containing planar triarylmethyl carbocations (Fig. 4e),[58,173] demonstrated that the fluorescence lifetime of DAOTA-M2 significantly changes upon interaction with different nucleic acid topologies. Specifically, its lifetime is prolonged when bound to G4s compared to double- or single-stranded nucleic acids. This enabled the first live-cell detection of G4s using FLIM[173] and facilitated studies investigating the unwinding effect of *FANCJ* and *RTEL1* on G4s.[58] Subsequent FLIM probes, such as the tricationic probe NBTE, based on photon counting, were used for quantitative detection of dG4s in cancer/normal cells and revealed that dG4s are four times more abundant in cancer cells than in normal cells, highlighting the potential of FLIM probes for cancer cell detection (Fig. 4g).[52] Additionally, rG4s have been studied using FLIM. TOR-G4, a probe derived from thiazole orange, primarily colocalizes with RNA in the cytoplasm and nucleolus, clarifying the distribution of rG4s and marking the first FLIM probe designed to study novel RNA functions in cells (Fig. 4f).[162] Phosphorescence, which has a longer lifetime than fluorescence, offers broader lifetime tuning capabilities and minimizes interference from sub-nanosecond biological fluorescence species in cells. Recently, a platinum(II) complex-based probe was developed for dG4s detection, exhibiting a higher affinity for G4s than other nucleic acid structures.[160] Upon binding to dG4s, this probe shows a significant increase in phosphorescence emission and a prolonged phosphorescence lifetime, representing the first phosphorescence lifetime imaging of G4s in live cells. In conclusion, FLIM methods address several limitations of basic fluorescence imaging, such as interference from local molecular concentrations and environmental factors like macromolecular crowding and viscosity in live-cell environments. FLIM offers a novel approach for distinguishing G4s from other nucleic acid structures in live cells, providing new insights into the molecular dynamics and interactions of G4s in cellular contexts.

Detection of G4 dynamic in cells

Abnormal expression of G4s has been associated with various diseases, including cancer and neurodegenerative disorders.[134,139,183] High levels of G4s are also observed in cells infected by certain bacteria and viruses.[51] The structural plasticity of G4s, particularly their ability to bind small molecules in diverse conformations, makes them a promising target for therapeutic intervention in these diseases. Therefore, understanding the folding dynamics and conformational changes of G4s in live cells is essential for elucidating their biological functions and developing G4-targeting drugs.

Several methods for the detection and functional study of G4s in live cells have been developed, primarily relying on ligands—such as antibodies or small-molecule probes—that specifically bind to or stabilize G4s. However, high concentrations of such ligands can lead to the global formation of G4 structures, potentially disrupting endogenous G4 folding dynamics and causing cellular stress or toxicity. To address this issue, the G4-specific fluorescent probe SiR-PyPDS has been developed (Fig. 5a).[184] This probe enables real-time, single-

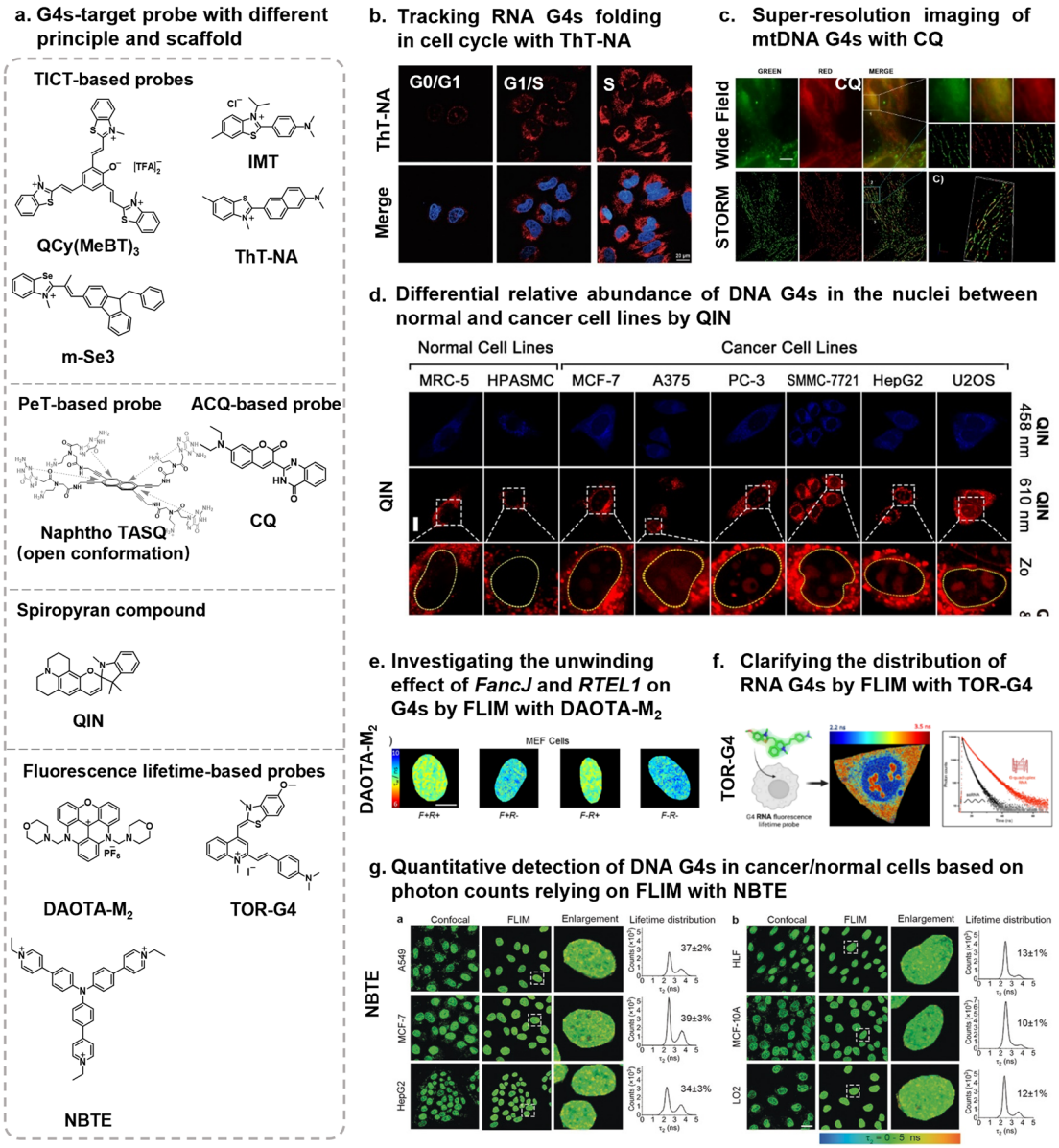

Fig. 4 Global Detection of G4s in cell. (a) G4s-target probes with different design principles and scaffolds. (b) Confocal imaging of synchronized HeLa cells at the G0/G1, G1/S, and S phase stained with ThT-NA (5 μM). Reproduced from ref. 55 with permission from American Chemical Society, copyright 2022. (c) Wide-field images and the reconstructed STORM images of live HepG2 cells co-stained with CQ and MitoTracker Red CMXRos and the amplified images. Scale bar: 10 μm. Reproduced from ref. 150 with permission from American Chemical Society, copyright 2022. (d) Confocal images of live cancer cells (U2OS, HepG2, SMMC-7721, PC-3, A375, and MCF-7) and normal cells (HPASMC and MRC5) co-stained with QIN (20 μM) and LysoTracker Green DND-26 (75 nM). Reproduced from ref. 181 with permission from American Chemical Society, copyright 2022. (e) FLIM map of G4s in MEF cells with altered FancJ and RTEL1 expression using DAOTA-M2. Reproduced from ref. 58 with permission from Wiley, copyright 2021. (f) FLIM images of TOR-G4 in U2OS cells, showing examples of cellular fluorescence decay and residuals from the decay fit. Reproduced from ref. 162 with permission from American Chemical Society, copyright 2024. (g) FLIM images of cancer cells (A549, MCF-7, and HepG2) and the corresponding normal cells (HLF, MCF-10A, and LO2) incubated with NBTE (20 mm, 24 h). Reproduced from ref. 52 with permission from Wiley, copyright 2020.

molecule imaging of individual dG4s folding events in live cells at low concentrations (20 nM) without interfering with G4 formation or dynamics. Single-molecule fluorescence imaging and time-dependent tracking of G4s in live cells have demonstrated that G4s fluctuate between folded and unfolded states. Furthermore, the study revealed that G4 formation in live cells is cell-cycle dependent, with the highest levels observed during the S phase and lower levels during the G1/S and G0/G1 phases, and that G4 folding can be terminated by methylation agents such as DMS. For rG4 folding dynamics, a red fluorescent probe based on a coumarin semisalicylamin scaffold, QUMA-1, has been shown to selectively dynamic track rG4s in live cells (Fig. 5b).[54] This probe has been used to track the dynamic folding process of rG4s under the influence of the RNA helicase

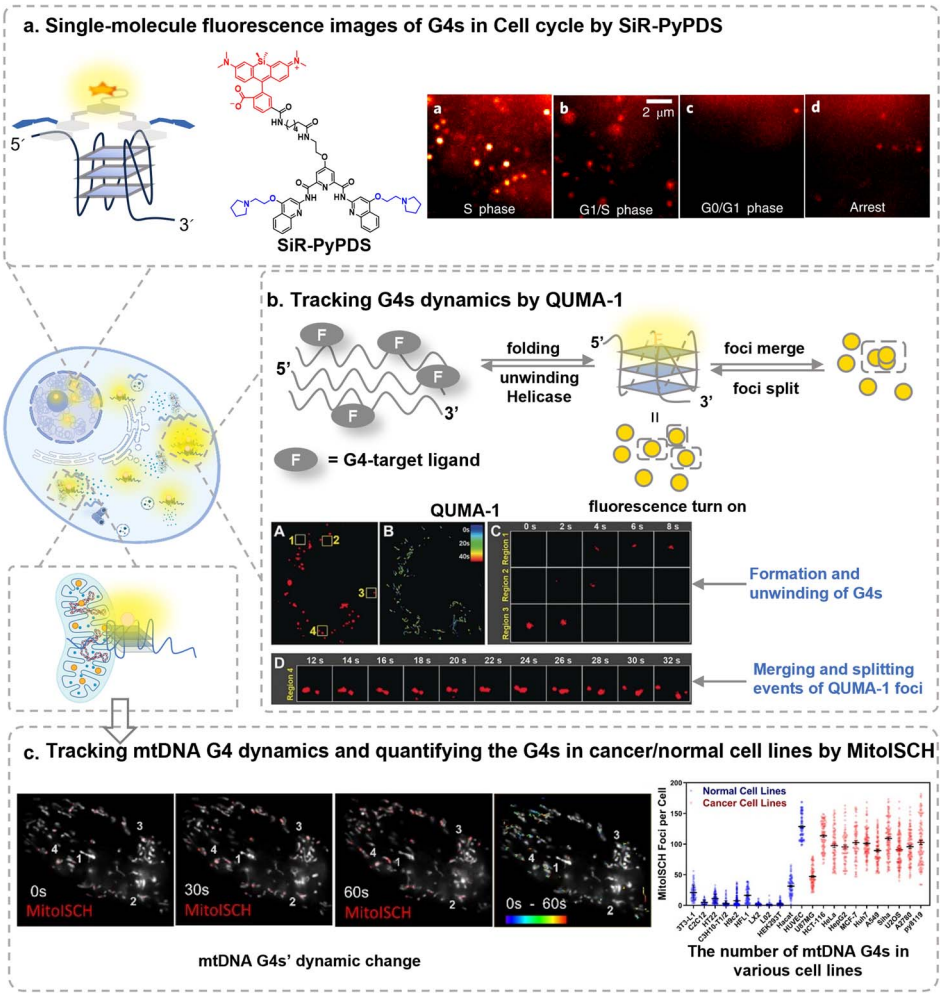

Fig. 5 The dynamic of G4s in live cells. (a) single-molecule fluorescence probe SiR-PyPDS was used to identify dynamic G4s during the cell cycle in the nucleus of live U2OS cells. Reproduced from ref. 184 with permission from Springer Nature, copyright 2020. (b) Imaging of G4s in live cells stained with QUMA-1. Putative G4 sequences can fold into G4 structures, and G4-targeting ligands bind to these structures, producing a fluorescent signal that can be used to locate G4s within the cell. Helicases can unwind G4 structures, leading to the disappearance of the fluorescence signal. Additionally, fluorescence foci can merge or split, potentially reflecting the assembly or disassembly of higher-order G4 structures. Reproduced from ref. 54 with permission from Wiley, copyright 2018. (c) Dynamics of mtDNA G4s, measured by the analysis of time-dependent movement and intensity of MitoISCH (1 μM) foci in live HeLa cells, imaged by structured illumination microscopy (SIM). MitoISCH, a G4-stabilizing agent, was used to monitor and modulate mtDNA G4s, revealing a link between mtDNA G4s and cell glycolysis. Reproduced from ref. 149 with permission from American Chemical Society, copyright 2021.

DHX36. The study observed that rG4s exhibit diffusion dynamics similar to RNA molecules and detected fluorescence signal merging and splitting, which may reflect the assembly or disassembly of higher-order G4 structures.

Mitochondria are essential organelles responsible for cellular energy metabolism. Recent research suggests that the folding and unwinding of mitochondrial DNA (mtDNA) G4s may be linked to mitochondrial genome instability and play a role in regulating mtDNA replication and transcription.[185–187] Investigating the folding dynamics of G4s in mitochondria can provide valuable insights into the abnormal behaviour of mitochondria in disease processes.[188] By fusing a lipophilic cationic triphenylphosphine group, responsive to mitochondrial membrane potential, with a dG4-targeting fluorescent probe, researchers have developed MitoISCH and MitoPDS[149] probes to monitor and regulate the dynamic changes of G4s in mitochondria (Fig. 5c). MitoISCH has been successfully used to track mtDNA G4s dynamic and quantify the G4s in cancer/normal cell lines. Notably, the study revealed that mtG4s are predominantly found in endothelial and cancer cells that rely on glycolysis. MitoPDS was shown to promote the folding of mtDNA G4s, which activated glycolysis-related genes and enhanced glycolytic activity. It provided the first evidence linking mtDNA G4s to the regulation of glycolysis, suggesting that they could serve as diagnostic targets for cancer and related metabolic diseases.

Furthermore, mtDNA is highly susceptible to oxidative damage (ROS) and is associated with age-related mutations and other forms of damage. To explore the role of G4s in oxidative damage and their folding states, researchers developed the CV2 peptide-based fluorescent probe, which utilizes depolymerization-induced emission to track G4 folding states.[66]

The CV2 probe demonstrates high specificity for parallel dG4 and strongly prefers mitochondria G4s over nuclear G4s. This probe has been effectively applied to monitor the folding states of G4s in mitochondria and to detect G4 loss due to oxidative damage induced by UV, MMS, or H_2O_2. The folding dynamics of G4s are complex, and small-molecule fluorescent probes such as CV2 offer novel opportunities to study these dynamics in detail. These tools hold significant potential for advancing research into the folding behaviours of G4s and their implications in cellular functions and disease mechanisms.

Detection of G4 topology in cell

The topology of G4s affects their thermal stability and the dynamics of their folding and unfolding, which are critical to their biological functions.[189] Developing fluorescent probes capable of selectively recognizing, stabilizing, or inducing specific G4s topologies is essential for elucidating the molecular mechanisms underlying the diverse roles of G4s conformations in cellular regulation. These structural differences influence the accessibility of the G4s edges and present opportunities for designing small-molecule probes that selectively target specific G4 conformations.

Most currently reported topology-specific G4s fluorescence probes target parallel G4 structures (Fig. 6a). For example, the ratio-based fluorescence probe NHCouI (Fig. 6b),[154] monitors nuclear changes during cell death processes by tracking dG4s formation, and QUMA-1,[54] which tracks rG4s folding and unwinding events in cancer cells. Additionally, ThT-NE has been employed to track the infection process of clinically isolated native HCV by visualizing its genomic G4s within the CG2 (Fig. 6c).[51] These probes generally contain at least two aromatic rings, and in solution, their fluorescence is quenched due to the TICT effect.

Accurately assessing the distribution of G4s *in vivo* is crucial for understanding G4-related diseases, such as cancer, and for developing targeted anticancer therapies. While most optical probes for detecting G4s in live cells emit in the visible light range (400–650 nm), these probes face significant challenges in live animal imaging, including tissue absorption, autofluorescence, and scattering, which limit their imaging depth. To address these limitations, our team developed a series of fluorescent protein mimics (igMFPs) based on a donor–acceptor–acceptor (D–A–A′) molecular configuration, capable of emitting tuneable fluorescence in the near-infrared (NIR) region. One such probe, NIR-2, binds to CG2a and exhibits a maximum emission wavelength of 689 nm (Fig. 6d).[159] This probe facilitates *in situ* visualization of rG4s within the HCV genome in mice model bearing GG2 cell-derived organoid and achieved high-contrast imaging of both HCV RNA and G4s *in vivo* for the first time. Furthermore, shifting the emission wavelength of G4 fluorescence probes into the NIR-II region significantly enhances imaging depth and contrast. A probe based on anthocyanin, NIRG-2, emits in the NIR-II range and, upon binding to G4s, effectively suppresses the free rotation of the donor group in NIRG-2 through multiple π–π interactions and hydrogen bonding.[175] This suppression reduces non-radiative transitions due to TICT and results in fluorescence activation (Em 950 nm). Compared to previously reported G4 probes, NIRG-2 not only enables high-resolution and high-contrast NIR-II fluorescence imaging of parallel G4 structures with a significant Stokes shift (90 nm) but also demonstrates excellent biocompatibility and photostability in live mice (Fig. 6e). NIRG-2 has been used to track oncogene-associated G4s for visualizing tumour lymphatic metastasis and, when combined with NIR-II fluorescence-guided precision resection, has proven effective in evaluating surgical and therapeutic outcomes in cancer metastasis models. While several small-molecule fluorescence probes targeting parallel G4 structures in live cells have been reported, probes for detecting antiparallel and hybrid G4s in live cells are rarely reported. More recently, McQuaid and Cardin's team developed a ruthenium complex, and NMR data confirmed that this probe binds specifically to single-molecule antiparallel chair-type G-quadruplexes.[190] This finding provides a structural basis for designing small-molecule probes to image antiparallel G4s.

Detection of sequence-specific G4s in cells using hybridization probe

The human genome contains a large number of putative G4 sequences, which, despite sharing similar folding dynamics, topological structures, and subcellular distributions, play distinct biological roles in both physiological and pathological processes.[15,60,191–194] Understanding the biological functions of specific G4 sequences and developing targeted G4-based therapeutics requires the development of probes that can specifically recognize G4s at the sequence or genomic locus level.[56] To address this need, Tan and colleagues pioneered the development of the first G4-induced hybridization probe *via* the G-quadruplex-triggered fluorogenic hybridization (GTFH) principle, named ISCH-NARS1. It was designed to detect the specific G4-rich sequence G4T25 in the 5′-UTR of NRAS mRNA. This probe consists of a complementary sequence to the terminal region of G4T25, coupled with the fluorophore ISCH-oa1 (Fig. 7a).[57] The oligonucleotide on ISCH-NRAS1 targets the terminal sequence of G4T25, guiding the fluorophore to bind selectively to the G4s of interest. Using a similar strategy, the team also developed the ISCH-MYC probe to visualize the stabilization and transition of c-*MYC* duplex–quadruplex structures, and the interactions between c-*MYC* DNA and associated proteins (Fig. 7b).[153] However, due to the low endogenous abundance of target G4s in cells, the GTFH probes are currently limited to detecting exogenously introduced sequences, restricting their use for *in situ* measurement of endogenous G4s.

Furthermore, the GTFH strategy relies primarily on fixed-cell *in situ* hybridization, limiting its applicability for dynamic duplex–quadruplex imaging in live cells. To overcome these limitations and enhance sensitivity, a modular multifunctional probe (MAMPA) was developed, combining rolling circle amplification (RCA) strategies to visualize endogenous rG4s in single genes within cells (Fig. 7c).[67] This probe consists of a G4

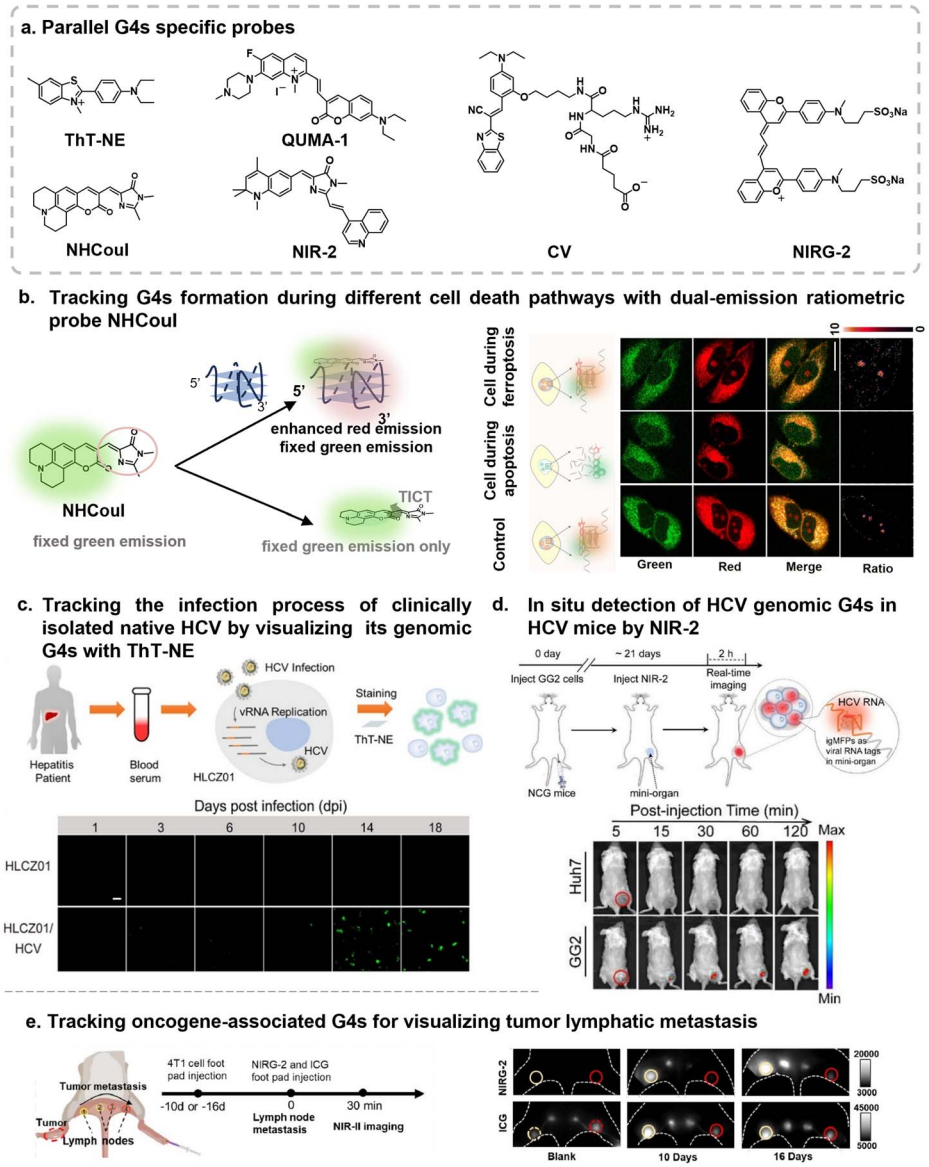

Fig. 6 Detection of typology-specific G4s in live cells and live mice. (a) Examples of probes specific to parallel G4s. (b) Ratiometric imaging using the dual-emissive probe NHCoul to track G4 formation during cell death pathways. The red emission of NHCoul specifically responds to parallel G4s, while its green emission serves as an inert internal reference signal for probe distribution. NHCoul can self-calibrate its signal, mitigating viscosity-induced interference within the major subcellular organelles during G4 imaging in live cells. Reproduced from ref. 154 with permission from Royal Society of Chemistry, copyright 2023. (c) Imaging of ThT-NE (1 μM)-stained HLCZ01 cells infected with hepatitis C patient serum, tracked from 1 to 18 days post-infection (dpi). Reproduced from ref. 51 with permission from American Chemical Society, copyright 2019. (d) Visualizing HCV rG4s by near-infrared fluorescence emissive probes NIR-2 *in vivo*. Reproduced from ref. 159 with permission from American Chemical Society, copyright 2021. (e) Schematic illustration of metastatic tumours in the lymph node with NIRG-2 and corresponding NIR-II fluorescence imaging of metastatic tumours in the lymph node after injection NIRG-2 or ICG (100 μM, 100 μL) 30 min. Reproduced from ref. 175 with permission from American Chemical Society, copyright 2024.

recognition module (ID-probe) and a signal amplification module (Amp-probe). The ID-probe first recognizes rG4s, while the Amp-probe targets RNA sequences adjacent to the rG4s. This interaction triggers a click reaction that couples the two modules. The complementary hybridization of the Amp-probe to the G4-adjacent sequence, followed by coupling between the modules, is a prerequisite for specific probe recognition. Subsequently, padlocks bind to the ID-probes, inducing their cyclization. Rolling circle amplification then uses the 3′ end of the Amp-probe sequence as a primer to generate a long RCA product starting from the circular DNA. This product can be visualized by hybridization with fluorescently labelled oligonucleotide probes, thus amplifying the target signal. This approach enables *in situ* imaging of G4s in individual genes (Fig. 7d). Through imaging rG4s in several individual genes, it was found that G4s were steadily occupied by G4s binding proteins (G4BPs) in various mRNAs in every cell line and defined “occupied G4s ratio”. It was shown that the proportion

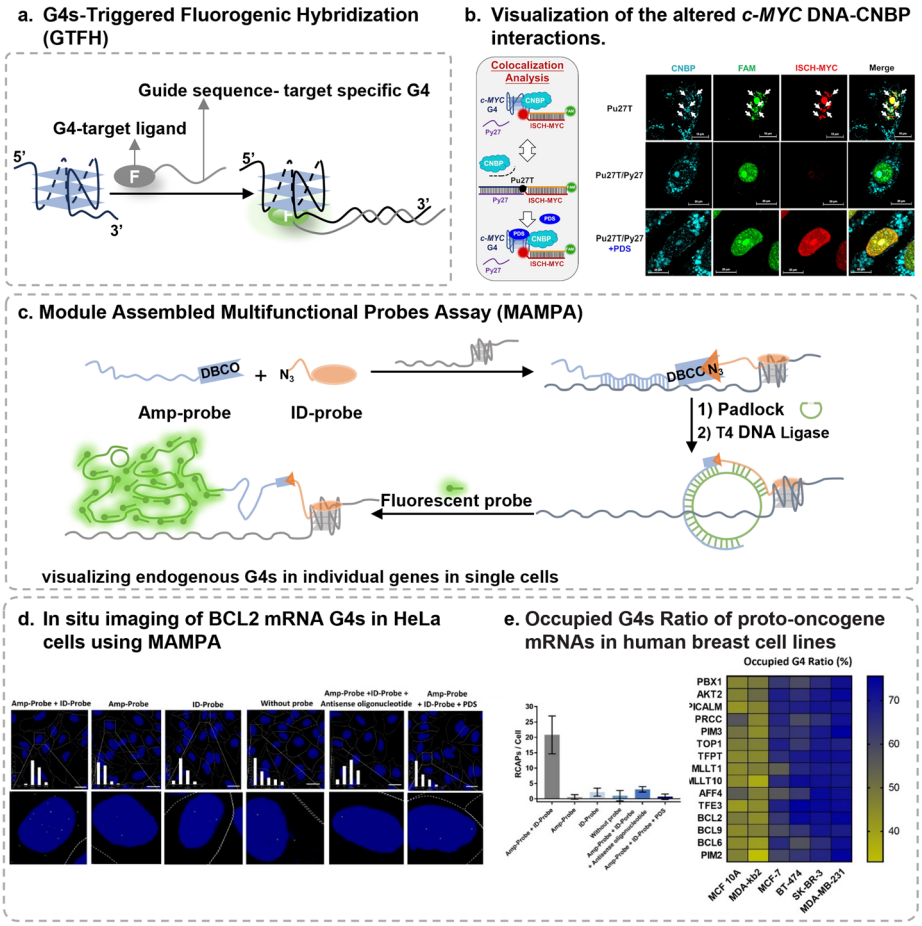

Fig. 7 Strategy for identifying sequence-specific G4s. (a) Scheme of GTFH. The sequence-specific probe consists of two components: a fluorescent "light-up" moiety that selectively binds to G4s and a guide sequence, which is a DNA molecule capable of hybridizing with a region adjacent to the guanine-rich sequence. (b) Immunofluorescence imaging of CNBP in Pu27T or Pu27T/Py27 transfected cells treated with or without PDS and then stained by ISCH-MYC. The DNAs are delivered into the nucleus by streptolysin O. White arrows indicate the distinct colocalization of FAM foci, CNBP foci, and "turn-on" ISCH-MYC signals. Reproduced from ref. 153 with permission from Oxford University Press, copyright 2022. (c) Scheme of MAMPA. ID-probes recognize rG4s through binding the G4-target ligand, while Amp-probes recognize specific RNA targets *via* complementary hybridization. ID-probes and Amp-probes are conjugated through a DBCO-N3 click reaction, templated by the targeted RNA. The ID probes then bind to padlocks, triggering cyclization to form circular DNA. Using Amp-probes as primers, RCA is initiated from the circular DNA, generating long RCA products. These products are subsequently visualized by hybridization with fluorophore-labelled oligonucleotide probes. (d) *In situ* imaging of BCL2 mRNA G4s in HeLa cells using MAMPA. Reproduced from ref. 67 with permission from Wiley, copyright 2022. (e) Occupied G4 ratio of proto-oncogene mRNAs in several human breast cell lines. Occupied G4 ratio is calculated by [1-RCAP (mRNA G4s)/RCAP (mRNAs)]. Reproduced from ref. 67 with permission from Wiley, copyright 2022.

of G4s associated with G4-binding proteins is higher in tumour cells than in normal cells, providing a novel method for studying the role of G4s in cancer cells and exploring their potential mechanisms in cancer and virus research (Fig. 7e).

Detection of G4 conformations in cells using NMR-based methods

The low abundance of endogenous G4s in live cells has traditionally posed a challenge for directly detecting G4 conformations using NMR. However, with the development of techniques such as mechanical microinjection,[45] streptolysin O (SLO)-induced pore formation,[195] and electroporation,[47,196] which enable the introduction of synthetic G4s into live cells, the concentration of G4-like molecules can be increased, making NMR-based detection of G4s in live cells more feasible (Fig. 8a and b). One study that employed SOFAST-HMQC (two-dimensional ^{1}H–^{15}N band-selective optimized flip-angle short-transient heteronuclear multiple quantum coherence) spectroscopy investigated the G4s model formed by four single-strand molecules of $d(TG_4T)_4$ in live *Xenopus laevis* oocytes.[64] This study demonstrated that the preferred conformation of G4s in the cellular environment closely resembles the conformation observed *in vitro* under potassium chloride conditions (Fig. 8c). Furthermore, this work marked the first demonstration that high-resolution NMR can directly study specific ligands targeting G4s within live cells.

To improve the sensitivity and accuracy of NMR detection in live cells, the chemical modification of nucleobases by incorporating heteronuclear atoms with high NMR signal sensitivity

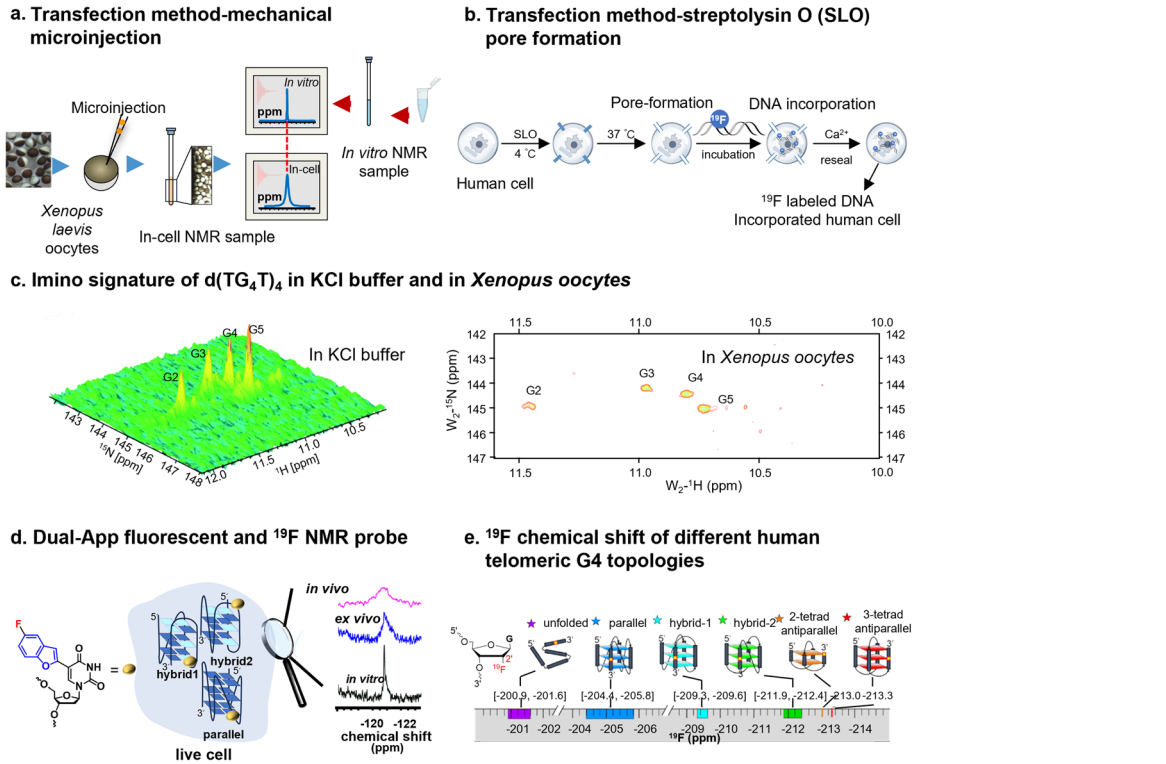

Fig. 8 Schematic overview of detection of G4s using NMR. (a) Mechanical microinjection transfects DNA into live *Xenopus laevis* oocytes. Reproduced from ref. 43 with permission from Oxford University Press, copyright 2017. (b) An SLO treatment-based transfection system is used to introduce DNA into HeLa cells. Reproduced from ref. 70 with permission from Oxford University Press, copyright 2019. (c) 2D imino signature of $d(TG_4T)_4$ in KCl buffer and *Xenopus* oocytes, acquired using a $^{1}H-^{15}N$ SOFAST-HMQC pulse sequence. Reproduced from ref. 64 with permission from Royal Society of Chemistry, copyright 2015. (d) Conformation-sensitive dual-app nucleoside analogue probe. This probe consists of a microenvironment-sensitive fluorophore and a ^{19}F label compatible with in-cell NMR. It can distinguish different G4s topologies and quantify topology-specific ligand binding using fluorescence and NMR techniques. Reproduced from ref. 197 with permission from American Chemical Society, copyright 2018. (e) Identification of the ^{19}F chemical shift fingerprint for human telomeric G4 topologies and the unfolded form by incorporating the commercial 2′-fluororiboguanosine (2′F-rG) at selected sites in 12 sequences known to fold into intramolecular G4s with well-defined topologies. Reproduced from ref. 41 with permission from American Chemical Society, copyright 2024.

has emerged as a promising strategy. Among these modifications, ^{19}F is particularly useful due to its high spin rate, chemical shift sensitivity to its environment, and absence of interference from endogenous fluorine.[42,63] As a result, ^{19}F NMR has been employed to study G4 structures in live cells. Using ^{19}F NMR, it was demonstrated that a 5′-fluoromethylphenyl-labeled human telomeric RNA G4 (r(UAGGGUAGGGU)) fragment, ORN-1, when introduced into *Xenopus* oocytes, formed higher-order G4 structures consisting of two stacked G4 subunits.[43,198] This study provided the first *in vivo* evidence of higher-order G4s in a cellular environment, revealing that these structures exhibit high thermal stability in a crowded solution.[43] Building on this approach, the same research group confirmed that telomeric DNA sequences in human cells (HeLa cells) could form two distinct hybrid-type and double-quadruplex antiparallel G4 structures, and DNA–RNA hybrid G4 structures.[70,199] Similarly, a fluorophore/NMR dual-responsive nucleoside analogue probe was developed by introducing conjugated fluorophenylfuran at the 5′ position of 2′-deoxyuridine. This probe enabled the identification of G4 conformations both *in vitro* and in native cellular environments (Fig. 8d).[197] The non-invasive nucleoside analogue was incorporated into human telomeric DNA oligonucleotide repeat sequences, facilitating the differentiation of various G4 topologies. The probe enabled the quantification of ligand-topology-specific binding through fluorescence and NMR techniques. It was found that telomeric DNA repeat sequences in live cells adopt hybrid and parallel G4 conformations without fully transitioning to a parallel structure. It contrasts with previous studies on G4s using immunofluorescence staining in fixed cells, as well as synthetic aggregation or crystallization conditions. These findings underscore the differences in the conformations adopted by nucleic acid motifs in complex cellular environments compared to non-natural conditions, highlighting the critical need for detecting G4 conformations in live cells.

Recently, Conggang Li's group developed a ^{19}F NMR chemical probe and conducted a quantitative study on the topology of G4s in human telomeric overhangs (Fig. 8e).[41] They found that longer overhang sequences tend to form stable G4 structures at both the 5′- and 3′-ends, whereas internal G4s exhibit more dynamic behaviours, "sliding" along the sequence and connecting through TTA or 1–3 TTAGGG repeats. These extended G4 overhang sequences induce conformational isomerism, with the predominant conformations at the 5′-end, internal region,

and 3′-end being hybrid-2, two- or three-tetrad antiparallel, and hybrid-1, respectively. Furthermore, different behaviours of telomeric sequences of varying lengths were observed in live cells, suggesting that overhang length and protein accessibility are linked to their functional roles. This technique provides a powerful tool for quickly identifying and quantifying the folding topology and relative abundance of long human telomeric overhangs. The results from 2D NMR and ^{19}F NMR experiments offer preliminary evidence that G4 conformations differ between *in vitro* and intracellular environments, underscoring the necessity of live-cell detection for studying G4 conformations. These findings provide critical insights into the biological functions of G4s and offer valuable guidance for designing G4-targeted anticancer and antitumor therapies based on G4-binding ligands.

Limitation and perspective

G4s have emerged as fundamental features within the genome, influencing and participating in a wide range of key biological processes. The need to unravel these biological insights continues to drive the development of advanced tools for G4 detection and imaging. However, many challenges still need to be addressed. This review highlights the primary biological functions of G4s and their involvement in various cellular processes. We have also discussed current methods for detecting G4s in cells, including global detection, folding conformation analysis using fluorescence and live-cell NMR, and sequence-specific G4 identification based on hybridization principles. Despite significant progress in live-cell G4 detection technologies, several challenges remain.

(1) How to detect G4s at key genomic loci in live cells

Current approaches for G4 detection primarily rely on recognizing G4 structural features. However, due to the structural similarities among different G4s, their interactions often lead to global interference, as G4s at multiple genomic loci exhibit similar conformations. This overlap complicates the precise identification of G4s in a complex cellular environment. Additionally, for clinical diagnostics and drug development, such probes may pose a risk to healthy cells with rapid turnover, such as those in intestinal and skin epithelia.[56]

Base-pairing complementary G4 probes have significantly advanced the ability to recognize specific G4 sequences within cells and genes. These probes provide a foundation for studying the interactions between particular G4 structures and their binding proteins, as well as for exploring how G4s regulate gene function and for the development of G4-targeted therapeutic agents. However, several challenges remain, including the low abundance of G4s in live cells and the limited penetration of probes across cell membranes, particularly when complementary sequences are introduced. Achieving *in situ* detection, signal amplification and even tracking of individual G4s, remains a significant hurdle.

Recent advances in peptide nucleic acids (PNAs) and locked nucleic acids (LNAs)—synthetic oligonucleotides comprising 2′,4′-hydroxyl-modified, methylene-bridged unnatural nucleotides—have attracted significant attention owing to their improved structural stability and enhanced cellular membrane permeability.[200–206] By chemically modifying their structures and combining them with high-brightness single-molecule fluorescence probes or self-assembling probes that target G4s, it may be possible to increase signal output while minimizing global interference from the probes. This approach offers significant potential for enabling sequence-specific G4 recognition in live cells, and developing G4-targeted drugs with minimal global interference, thereby providing new opportunities for both G4 detection and therapeutic development.

Besides, new G4 recognition strategies, including fusion recognition models, have been developed, offering promising avenues for G4 detection. One such approach involves L-RNA aptamers, formed by artificial, single-stranded mirror L-RNA nucleotides. These aptamers primarily recognize G4 structures through their three-dimensional conformations, and they have been shown to regulate protein expression by interacting with G4s in the 5′ untranslated region (UTR).[207] Importantly, L-RNA aptamers do not engage in Watson–Crick base pairing with natural D-nucleotides and are resistant to nuclease degradation. Furthermore, L-RNA aptamers can tolerate various chemical modifications, enhancing their targeting efficiency, pharmacokinetics, and stability in biological environments.[208] These aptamers can also be endowed with fluorescent emission capabilities by incorporating specific chemical modifications, potentially expanding their utility in studying G4 dynamics.

Significantly, CRISPR (clustered regularly interspaced short palindromic repeats) technology, when fused with catalytically inactive nucleases, allows for the alteration of small guide RNAs (sgRNAs) to target specific sequences.[209] This enables the recruitment of functional proteins or compounds to particular loci.[210–212] Recent studies have coupled dCas9 with G4-binding proteins, such as nucleolin, or G4-stabilizing ligands like PDS, to successfully stabilize G4s at key genomic loci, including promoters of oncogenes like *MYC*, muscle-associated genes such as *Itga7*, and telomere-associated G4s. This stabilization leads to cellular outcomes such as proliferation arrest, inhibition of myogenic differentiation, and cellular senescence.[213] These studies provide new insights into the targeted manipulation of G4s in live cells and hold promise for developing drugs with minimized off-target effects.

(2) How to detect G4s quantitatively in live cells

Significant progress has been made in the qualitative analysis of G4 folding, distribution, and abundance in live cells using G4-targeted fluorescence probes. However, several challenges remain in achieving semi-quantitative or quantitative analysis of G4's dynamic expression under specific physiological conditions in live cells. It is significant for establishing a clear relationship between G4s and downstream biological functions. While fluorescence intensity-based comparisons can provide qualitative insights into the relative abundance of G4s under different physiological conditions, the potential G4-induced effects of probes and the nonlinear relationship between

fluorescence output and G4 abundance in live cells hinder more accurate semi-quantitative analysis. Fluorescent lifetime-based probes generally do not require high-affinity binding to G4s, making them less prone to G4-induced effects and more resistant to interference from complex cellular environments. TCSPC-FLIM has emerged as a feasible technique for quantitatively analysing G4 levels in live cells based on photon counts. However, while TCSPC-FLIM offers high fluorescence lifetime resolution, it is limited by its low spatiotemporal resolution, primarily due to prolonged sampling times. This limitation hampers dynamic imaging and the quantitative analysis of G4 folding events.

Recently, frequency-domain phase-shift FLIM (phase-FLIM) has shown potential for dynamic imaging and super-resolution applications. Developing small-molecule probes with well-defined lifetime responsiveness has become a key area of exploration in this context.[214] Furthermore, ratio-based fluorescence probes have demonstrated promise for G4 quantification. However, these probes currently suffer from a narrow range of ratio values, which limits their utility. Therefore, rational molecular design is critical in optimizing the emission intensities between the two fluorophores. Expanding the linear response range of the G4 ratio will be essential for enabling the application of these probes in quantitative studies of G4s in live cells.

(3) How to detect the dynamic conformation of intrinsic G4s in live cells

The development of topology-specific probes and NMR tools for G4s in live cells has enabled the investigation of G4 conformations in their native cellular environment. However, due to the relatively low abundance of G4s in live cells, structural studies under physiological conditions typically require the exogenous introduction of G4 sequences to enhance their concentration and signal response. This approach risks introducing artifacts, as the non-physiological concentrations of G4s may not accurately reflect their native cellular conditions. Additionally, the low sensitivity of NMR presents a significant challenge for directly determining the structure of G4s *in situ* within live cells. The long sampling times required for NMR studies can also negatively impact cellular viability and nucleic acid sequences' stability, further complicating the analysis of G4 conformations in live cells.

Nevertheless, in the long term, cellular NMR and other structural methods are expected to be pivotal in addressing fundamental biological questions. A major hurdle remains: how to identify native G4 conformations in live cells and design small molecules that specifically recognize G4 conformations and loops based on the plasticity of G4-ligand interactions. This area requires further investigation and refinement. Recent advancements in combining dynamic nuclear polarization (DNP) and parahydrogen-induced polarization (PHIP) strategies with ^{13}C and ^{15}N isotope labelling at key sites show promise for improving the study of G4s and nucleic acid folding dynamics,[64,215,216] including aptamers, in live cells. Moreover, starting with the conformation analysis of G4s obtained *via* cellular NMR, integrating artificial intelligence (AI) models focused on nucleic acid-small molecule interactions may provide new avenues for designing topology-specific small molecules that target G4s effectively.[217,218]

(4) How to detect subcellular localized G4s in live cells

Current research primarily focuses on G4s in the cell nucleus and their biological functions, with comparatively limited attention given to other subcellular compartments. For example, the unique circular DNA structure, replication mechanisms, and high K^+ concentrations in mitochondria create an environment conducive to G4 formation.[185] The presence or aberrant expression of G4s in mitochondria can significantly affect mitochondrial energy production. However, studies on mtDNA G4s remain primarily limited to sporadic identification and preliminary dynamic analyses. Ribosomal RNA (rRNA), produced in the nucleolus, accounts for approximately 82% of the total RNA in the cell and is rich in GC-rich sequences. It plays a pivotal role in cell proliferation and regulating essential cellular processes. Thus, developing small-molecule ligand probes that specifically target dG4s and rG4s in different subcellular regions and studying their interactions with functional proteins is crucial for understanding their biological roles and elucidating connections between nucleic acids and epigenetic regulation. One promising strategy involves adapting existing methods for studying nuclear or global G4s to rationally design small-molecule probes with chemically modified structures that can control their subcellular localization.[58,149,152] This approach can potentially deepen our understanding of G4s and their functional implications across various cellular contexts.

(5) How to detect G4s in live animals

The significantly higher abundance of G-quadruplexes (G4s) in various tumour cells compared to normal cells makes them promising molecular biomarkers for early cancer diagnosis.[67,219] Developing *in vivo* G4s detection technology holds crucial clinical value for early tumour identification and intervention, particularly in detecting micro-lesions, which could effectively prevent disease progression. Furthermore, the development of G4s-based *in vivo* imaging tools may provide real-time navigation for precision tumour surgery, potentially improving the accuracy of tumour resection and therapeutic outcomes. However, limited optical penetration depth and sensitivity of most currently available fluorescence molecules in the visible light wavelength constrain their use in clinical *in situ* diagnostics for G4s. The near-infrared (NIR) fluorescence window (650–900 nm) minimizes light absorption by haemoglobin and water, while the NIR-II fluorescence window (1000–1700 nm) further reduces photon scattering, making it ideally suited for *in vivo* imaging. Recently, the development of G4 probes with NIR and NIR-II emission capabilities has enabled the detection of G4s in live animals, opening up new opportunities for clinical applications, such as disease biopsy analyses targeting G4s.[220]

Several strategies can be employed to design probes with longer emission wavelengths and higher brightness. Extending the conjugation system of the probe can effectively increase

both the absorption and emission wavelengths.[221,222] For probes that rely on intramolecular charge transfer (ICT), optimizing the electron-donating and electron-accepting abilities of donor/acceptor units and reducing the energy gap between the HOMO and LUMO orbitals can improve ICT efficiency, thereby extending emission wavelengths.[223] Additionally, introducing other photophysical mechanisms, such as excited-state intramolecular proton transfer (ESIPT), offers further advantages. ESIPT-based fluorophores exhibit substantial Stokes shifts (approximately 200 nm), effectively redshirting the emission wavelength.[224] On the other hand, improving the quantum yield and molar extinction coefficient of the probes can further enhance their brightness.[224–226] Strategies include incorporating rigid structures into the probe to reduce vibrational bond flexibility, minimizing non-radiative transitions that lead to energy loss,[221] and introducing shielding units to protect the probe from solvent interference.[226] Enhancing the molar extinction coefficient can be achieved by incorporating structural units with high absorptivity or modifying the probe with donor or acceptor groups to optimize electron distribution, thereby enhancing photon capture capabilities, such as BODIPY and rhodamine derivatives.[227–233]

Beyond the optical approaches, in clinical practice, molecular imaging techniques such as single-photon emission computed tomography (SPECT) and positron emission tomography-computed tomography (PET-CT) are commonly employed for *in vivo* diagnostics.[234,235] Recently, a SPECT study using a block of platinum(II)–salphen complex labelled with the radioactive isotope ^{111}In to target G4s demonstrated that, due to low cellular uptake, the observed *in vivo* signal was primarily attributed to tissue accumulation, rather than specific G4 targeting.[236] Optimizing the chemical structure of molecular tracers to enhance their *in vivo* metabolism and cell membrane penetration could provide valuable avenues for future research.

(6) How to detect disease-associated G4s in live cells

Advances in G4 recognition have enabled real-time, high-contrast imaging of the HCV genome in live cells and live animals. *In vitro* studies have also demonstrated the mechanisms of certain neurodegenerative diseases such as Huntington's disease (HD), fragile X syndrome, amyotrophic lateral sclerosis (ALS), and frontotemporal dementia (FTD) caused by nucleotide repeat expansions.[134,141,144] However, research on disease-specific G4s remains incomplete, leaving many areas worth exploring. For example, G4s have been identified in the genomes of viruses within the Retroviridae family, such as human immunodeficiency virus (HIV), as well as herpesviruses, and members of the Flaviviridae family, including Zika virus, Ebola virus (EBOV), and Marburg virus. Rapidly identifying these viral G4s in the clinic and developing therapeutic strategies targeting them remain critical areas for further investigation. It requires developing G4 detection tools that can avoid misdiagnoses caused by aberrant G4s that may arise in non-disease states or other unrelated conditions. Accurate localization and characterization of G4s in different diseases are therefore critical for providing reliable diagnostic and therapeutic frameworks.

Relying on existing probe technologies and conventional imaging methods (*e.g.*, antibody-based tissue staining or live fluorescence imaging), *in vivo* ensemble G4s detection shows potential for rapidly evaluating the correlation between global G4 distribution and pathological phenotypes (such as tumour progression or neurodegenerative diseases). These approaches can provide a macroscopic foundation for clinical diagnosis and preliminary drug screening. In contrast, *in situ* single-molecule detection of G4s *in vivo* poses more significant technical challenges, requiring the mitigation of background noise, improved targeting specificity of probes, and enhanced stability for long-term dynamic monitoring. Yet, such techniques can uncover the folding dynamics, conformational heterogeneity, and transient interaction mechanisms of individual G4 structures with target proteins—insights critical for precisely elucidating G4-related pathological roles and developing highly specific therapeutics. Future research should adopt a dual-track strategy: (1) optimizing ensemble G4s detection tools to enable high-throughput clinical translation; (2) breaking the bottlenecks of *in vivo* single-molecule imaging by integrating multimodal probe design and *in vivo*-compatible super-resolution imaging. It will bridge the gap from "macroscopic correlation" to "microscopic mechanism", ultimately advancing precision and personalized G4-targeted therapies.

In summary, this perspective offers a comprehensive overview of the progressively refined tools for G4 detection, from single-molecule resolution to live-cell and *in vivo* applications. It highlights the advancements in understanding the increasingly complex biological functions of G4s, from static structures to dynamic processes. We have introduced the applications of these methods in functional studies, discussed the current challenges in G4 detection, and explored potential solutions. We hope this perspective will help researchers better understand both the potential and limitations of existing G4 detection tools. Furthermore, it aims to provide theoretical guidance for the rational design and development of tools dedicated to studying G4 functions and elucidating the links between G4s and diseases. We also hope this perspective will inspire more researchers to engage in this field, bringing new ideas and perspectives to advance the application of G4 detection methods in disease diagnosis and targeted therapies.

Data availability

This perspective does not contain any original data. All the data presented in this perspective have been sourced from publicly available research studies and data published in peer-reviewed journals.

Author contributions

H. L. was responsible for conducting the literature review and drafting the initial manuscript. Z. J. was responsible for preparing images. S. G. and C. L. helped to revise the manuscript. S. K. was instrumental in conceiving the overarching

concept, contributing to the overall planning, and participating in the writing processes. Z. N. was engaged in the overarching concept and editing processes.

Conflicts of interest

There are no conflicts to declare.

Acknowledgements

This work was supported by the National Key R&D Program of China (2024YFA0916700), the National Natural Science Foundation of China (22034002, 92253304, 22274041, and 22204047), the Natural Science Foundation of Hunan Province (2023ZJ1123, 2024RC3091 and 2023JJ40122) and the Fundamental Research Funds for the Central Universities.

Notes and references

1 J. Choi and T. Majima, *Chem. Soc. Rev.*, 2011, **40**, 5893.
2 P. Sarkies, C. Reams, L. J. Simpson and J. E. Sale, *Mol. Cell*, 2010, **40**, 703–713.
3 A. Siddiqui-Jain, C. L. Grand, D. J. Bearss and L. H. Hurley, *Proc. Natl. Acad. Sci. U. S. A.*, 2002, **99**, 11593–11598.
4 H. Técher, S. Koundrioukoff, A. Nicolas and M. Debatisse, *Nat. Rev. Genet.*, 2017, **18**, 535–550.
5 S. De and F. Michor, *Nat. Struct. Mol. Biol.*, 2011, **18**, 950–955.
6 T. De Lange, *Nat. Rev. Mol. Cell Biol.*, 2004, **5**, 323–329.
7 P. Agarwala, S. Pandey and S. Maiti, *Org. Biomol. Chem.*, 2015, **13**, 5570–5585.
8 P. Kharel, S. Balaratnam, N. Beals and S. Basu, *Wiley Interdiscip. Rev.: RNA*, 2020, **11**, e1568.
9 D. Varshney, J. Spiegel, K. Zyner, D. Tannahill and S. Balasubramanian, *Nat. Rev. Mol. Cell Biol.*, 2020, **21**, 459–474.
10 G. Guilbaud, P. Murat, B. Recolin, B. C. Campbell, A. Maiter, J. E. Sale and S. Balasubramanian, *Nat. Chem.*, 2017, **9**, 1110–1117.
11 M. Gellert, M. N. Lipsett and D. R. Davies, *Proc. Natl. Acad. Sci. U. S. A.*, 1962, **48**, 2013–2018.
12 S. Burge, G. N. Parkinson, P. Hazel, A. K. Todd and S. Neidle, *Nucleic Acids Res.*, 2006, **34**, 5402–5415.
13 J. T. Davis, *Angew. Chem., Int. Ed.*, 2004, **43**, 668–698.
14 H. You, X. Zeng, Y. Xu, C. J. Lim, A. K. Efremov, A. T. Phan and J. Yan, *Nucleic Acids Res.*, 2014, **42**, 8789–8795.
15 J. L. Huppert and S. Balasubramanian, *Nucleic Acids Res.*, 2005, **33**, 2908–2916.
16 S. A. Dvorkin, A. I. Karsisiotis and M. Webba Da Silva, *Sci. Adv.*, 2018, **4**, eaat3007.
17 J. Kypr, I. Kejnovska, D. Renciuk and M. Vorlickova, *Nucleic Acids Res.*, 2009, **37**, 1713–1725.
18 Y. Geng, C. Liu, B. Zhou, Q. Cai, H. Miao, X. Shi, N. Xu, Y. You, C. P. Fung, R. U. Din and G. Zhu, *Nucleic Acids Res.*, 2019, **47**, 5395–5404.
19 V. S. Chambers, G. Marsico, J. M. Boutell, M. Di Antonio, G. P. Smith and S. Balasubramanian, *Nat. Biotechnol.*, 2015, **33**, 877–881.
20 C. K. Kwok, G. Marsico, A. B. Sahakyan, V. S. Chambers and S. Balasubramanian, *Nat. Methods*, 2016, **13**, 841–844.
21 T. Liu, X. Shen, Y. Ren, H. Lu, Y. Liu, C. Chen, L. Yu and Z. Xue, *eLife*, 2024, **13**, RP99026.
22 Y. Feng, S. Tao, P. Zhang, F. R. Sperti, G. Liu, X. Cheng, T. Zhang, H. Yu, X. Wang, C. Chen, D. Monchaud and W. Zhang, *Plant Physiol.*, 2022, **188**, 1632–1648.
23 H. B. Cagirici and T. Z. Sen, *G3: Genes, Genomes, Genet.*, 2020, **10**, 2021–2032.
24 M. Dobrovolná, N. Bohálová, V. Peška, J. Wang, Y. Luo, M. Bartas, A. Volná, J.-L. Mergny and V. Brázda, *Int. J. Mol. Sci.*, 2022, **23**, 8482.
25 R. Perrone, M. Nadai, I. Frasson, J. A. Poe, E. Butovskaya, T. E. Smithgall, M. Palumbo, G. Palù and S. N. Richter, *J. Med. Chem.*, 2013, **56**, 6521–6530.
26 S.-R. Wang, Y.-Q. Min, J.-Q. Wang, C.-X. Liu, B.-S. Fu, F. Wu, L.-Y. Wu, Z.-X. Qiao, Y.-Y. Song, G.-H. Xu, Z.-G. Wu, G. Huang, N.-F. Peng, R. Huang, W.-X. Mao, S. Peng, Y.-Q. Chen, Y. Zhu, T. Tian, X.-L. Zhang and X. Zhou, *Sci. Adv.*, 2016, **2**, e1501535.
27 A. M. Fleming, Y. Ding, A. Alenko and C. J. Burrows, *ACS Infect. Dis.*, 2016, **2**, 674–681.
28 P. Krafčíková, E. Demkovičová and V. Víglaský, *Biochim. Biophys. Acta, Gen. Subj.*, 2017, **1861**, 1321–1328.
29 J. U. Guo and D. P. Bartel, *Science*, 2016, **353**, aaf5371.
30 F. Kouzine, D. Wojtowicz, L. Baranello, A. Yamane, S. Nelson, W. Resch, K.-R. Kieffer-Kwon, C. J. Benham, R. Casellas, T. M. Przytycka and D. Levens, *Cell Syst.*, 2017, **4**, 344–356.
31 J. R. Williamson, M. K. Raghuraman and T. R. Cech, *Cell*, 1989, **59**, 871–880.
32 K. A. Wilkinson, E. J. Merino and K. M. Weeks, *Nat. Protoc.*, 2006, **1**, 1610–1616.
33 J. Kypr, I. Kejnovska, D. Renciuk and M. Vorlickova, *Nucleic Acids Res.*, 2009, **37**, 1713–1725.
34 J. Carvalho, J. A. Queiroz and C. Cruz, *J. Chem. Educ.*, 2017, **94**, 1547–1551.
35 R. del Villar-Guerra, J. O. Trent and J. B. Chaires, *Angew. Chem., Int. Ed.*, 2018, **57**, 7171–7175.
36 K. McQuaid, H. Abell, S. P. Gurung, D. R. Allan, G. Winter, T. Sorensen, D. J. Cardin, J. A. Brazier, C. J. Cardin and J. P. Hall, *Angew. Chem., Int. Ed.*, 2019, **58**, 9881–9885.
37 F. Guarra, T. Marzo, M. Ferraroni, F. Papi, C. Bazzicalupi, P. Gratteri, G. Pescitelli, L. Messori, T. Biver and C. Gabbiani, *Dalton Trans.*, 2018, **47**, 16132–16138.
38 L. Y. Lin, S. McCarthy, B. M. Powell, Y. Manurung, I. M. Xiang, W. L. Dean, B. Chaires and L. A. Yatsunyk, *PLoS One*, 2020, **15**, e0241513.
39 G. R. Clark, P. D. Pytel, C. J. Squire and S. Neidle, *J. Am. Chem. Soc.*, 2003, **125**, 4066–4067.
40 G. N. Parkinson and G. W. Collie, in *G-Quadruplex Nucleic Acids*, ed. D. Yang and C. Lin, Springer New York, New York, NY, 2019, vol. 2035, pp. 131–155.

41 C. Wang, G. Xu, X. Liu, L. Jiang, X. Zhou, M. Liu and C. Li, *J. Am. Chem. Soc.*, 2024, **146**, 4741–4751.
42 H. Chen, S. Viel, F. Ziarelli and L. Peng, *Chem. Soc. Rev.*, 2013, **42**, 7971.
43 H.-L. Bao, T. Ishizuka, T. Sakamoto, K. Fujimoto, T. Uechi, N. Kenmochi and Y. Xu, *Nucleic Acids Res.*, 2017, **45**, 5501–5511.
44 P. Broft, S. Dzatko, M. Krafcikova, A. Wacker, R. Hänsel-Hertsch, V. Dötsch, L. Trantirek and H. Schwalbe, *Angew. Chem., Int. Ed.*, 2021, **60**, 865–872.
45 M. Krafcikova, R. Hänsel-Hertsch, L. Trantirek and S. Foldynova-Trantirkova, in *G-Quadruplex Nucleic Acids*, ed. D. Yang and C. Lin, Springer New York, New York, NY, 2019, vol. 2035, pp. 397–405.
46 A. Criscuolo, E. Napolitano, C. Riccardi, D. Musumeci, C. Platella and D. Montesarchio, *Pharmaceutics*, 2022, **14**, 2361.
47 M. Krafcikova, S. Dzatko, C. Caron, A. Granzhan, R. Fiala, T. Loja, M.-P. Teulade-Fichou, T. Fessl, R. Hänsel-Hertsch, J.-L. Mergny, S. Foldynova-Trantirkova and L. Trantirek, *J. Am. Chem. Soc.*, 2019, **141**, 13281–13285.
48 *NMR of Biomolecules: Towards Mechanistic Systems Biology*, ed. I. Bertini, K. S. McGreevy and G. Parigi, Wiley, 1st edn, 2012.
49 M. Adrian, B. Heddi and A. T. Phan, *Methods*, 2012, **57**, 11–24.
50 C. Dalvit, G. Fogliatto, A. Stewart and M. Veronesi, *J. Biomol. NMR*, 2001, **21**, 349–359.
51 X. Luo, B. Xue, G. Feng, J. Zhang, B. Lin, P. Zeng, H. Li, H. Yi, X.-L. Zhang, H. Zhu and Z. Nie, *J. Am. Chem. Soc.*, 2019, **141**, 5182–5191.
52 L. Liu, W. Liu, K. Wang, B. Zhu, X. Xia, L. Ji and Z. Mao, *Angew. Chem., Int. Ed.*, 2020, **59**, 9719–9726.
53 F. Rota Sperti, J. Mitteaux, J. Zell, A. Pipier, I. E. Valverde and D. Monchaud, *RSC Chem. Biol.*, 2023, **4**, 456–465.
54 X. Chen, S. Chen, J. Dai, J. Yuan, T. Ou, Z. Huang and J. Tan, *Angew. Chem., Int. Ed.*, 2018, **57**, 4702–4706.
55 X. Lu, X. Wu, S. Kuang, C. Lei and Z. Nie, *Anal. Chem.*, 2022, **94**, 10283–10290.
56 E. Cadoni, L. De Paepe, A. Manicardi and A. Madder, *Nucleic Acids Res.*, 2021, **49**, 6638–6659.
57 S.-B. Chen, M.-H. Hu, G.-C. Liu, J. Wang, T.-M. Ou, L.-Q. Gu, Z.-S. Huang and J.-H. Tan, *J. Am. Chem. Soc.*, 2016, **138**, 10382–10385.
58 P. A. Summers, B. W. Lewis, J. Gonzalez-Garcia, R. M. Porreca, A. H. M. Lim, P. Cadinu, N. Martin-Pintado, D. J. Mann, J. B. Edel, J. B. Vannier, M. K. Kuimova and R. Vilar, *Nat. Commun.*, 2021, **12**, 162.
59 T. Santos, G. F. Salgado, E. J. Cabrita and C. Cruz, *Pharmaceuticals*, 2021, **14**, 769.
60 G. Biffi, D. Tannahill, J. McCafferty and S. Balasubramanian, *Nat. Chem.*, 2013, **5**, 182–186.
61 A. Laguerre, K. Hukezalie, P. Winckler, F. Katranji, G. Chanteloup, M. Pirrotta, J.-M. Perrier-Cornet, J. M. Y. Wong and D. Monchaud, *J. Am. Chem. Soc.*, 2015, **137**, 8521–8525.
62 S. Manna and S. G. Srivatsan, *RSC Adv.*, 2018, **8**, 25673–25694.
63 E. Luchinat, M. Cremonini and L. Banci, *Chem. Rev.*, 2022, **122**, 9267–9306.
64 G. F. Salgado, C. Cazenave, A. Kerkour and J.-L. Mergny, *Chem. Sci.*, 2015, **6**, 3314–3320.
65 P. Yin, C. Huang, L. Zhang, Z. Li, C. Zhong, S. Kuang, C. Lei, Y. Huang and Z. Nie, *Angew. Chem., Int. Ed.*, 2025, **64**, e202424060.
66 A. Pandith, Y. Luo, Y. Jang, J. Bae and Y. Kim, *Angew. Chem., Int. Ed.*, 2023, **62**, e202215049.
67 Y. Dai, X. Teng and J. Li, *Angew. Chem., Int. Ed.*, 2022, **61**, e202111132.
68 Z. Lu, S. Xie, H. Su, S. Han, H. Huang and X. Zhou, *Nucleic Acids Res.*, 2024, **52**, e37.
69 H. Su, J. Xu, Y. Chen, Q. Wang, Z. Lu, Y. Chen, K. Chen, S. Han, Z. Fang, P. Wang, B.-F. Yuan and X. Zhou, *J. Am. Chem. Soc.*, 2021, **143**, 1917–1923.
70 H.-L. Bao, H. Liu and Y. Xu, *Nucleic Acids Res.*, 2019, **47**, 4940–4947.
71 A. Korsakova and A. T. Phan, *NAR: Genomics Bioinf.*, 2023, **5**, lqad071.
72 L. Chen, J. Dickerhoff, S. Sakai and D. Yang, *Acc. Chem. Res.*, 2022, **55**, 2628–2646.
73 J. Han, M. Ge, P. Chen, S. Kuang and Z. Nie, *Biopolymers*, 2022, **113**, e23528.
74 E. Cadoni, L. De Paepe, A. Manicardi and A. Madder, *Nucleic Acids Res.*, 2021, **49**, 6638–6659.
75 V. Esposito, A. Galeone, L. Mayol, G. Oliviero, A. Virgilio and L. Randazzo, *Nucleosides, Nucleotides Nucleic Acids*, 2007, **26**, 1155–1159.
76 A. Guédin, J. Gros, P. Alberti and J.-L. Mergny, *Nucleic Acids Res.*, 2010, **38**, 7858–7868.
77 K. Lyu, E. Y.-C. Chow, X. Mou, T.-F. Chan and C. K. Kwok, *Nucleic Acids Res.*, 2021, **49**, 5426–5450.
78 A. Bugaut and S. Balasubramanian, *Biochemistry*, 2008, **47**, 689–697.
79 A. Arora, D. R. Nair and S. Maiti, *FEBS J.*, 2009, **276**, 3628–3640.
80 A. Joachimi, A. Benz and J. S. Hartig, *Bioorg. Med. Chem.*, 2009, **17**, 6811–6815.
81 A. Y. Q. Zhang, A. Bugaut and S. Balasubramanian, *Biochemistry*, 2011, **50**, 7251–7258.
82 D.-H. Zhang, T. Fujimoto, S. Saxena, H.-Q. Yu, D. Miyoshi and N. Sugimoto, *Biochemistry*, 2010, **49**, 4554–4563.
83 D. Bhattacharyya, G. Mirihana Arachchilage and S. Basu, *Front. Chem.*, 2016, **4**, 38.
84 H. Guiset Miserachs, D. Donghi, R. Börner, S. Johannsen and R. K. O. Sigel, *J. Biol. Inorg. Chem.*, 2016, **21**, 975–986.
85 G. Collie, A. P. Reszka, S. M. Haider, V. Gabelica, G. N. Parkinson and S. Neidle, *Chem. Commun.*, 2009, 7482.
86 M. Di Antonio, G. Biffi, A. Mariani, E. Raiber, R. Rodriguez and S. Balasubramanian, *Angew. Chem., Int. Ed.*, 2012, **51**, 11073–11078.
87 O. Mendoza, A. Bourdoncle, J.-B. Boulé, R. M. Brosh and J.-L. Mergny, *Nucleic Acids Res.*, 2016, **44**, 1989–2006.

88 M. M. Fay, S. M. Lyons and P. Ivanov, *J. Mol. Biol.*, 2017, **429**, 2127–2147.
89 E. Puig Lombardi and A. Londoño-Vallejo, *Nucleic Acids Res.*, 2020, **48**, 1–15.
90 J. L. Huppert and S. Balasubramanian, *Nucleic Acids Res.*, 2005, **33**, 2908–2916.
91 O. Kikin, L. D'Antonio and P. S. Bagga, *Nucleic Acids Res.*, 2006, **34**, W676–W682.
92 E. Belmonte-Reche and J. C. Morales, *NAR: Genomics Bioinf.*, 2020, **2**, lqz005.
93 A. B. Sahakyan, V. S. Chambers, G. Marsico, T. Santner, M. Di Antonio and S. Balasubramanian, *Sci. Rep.*, 2017, **7**, 14535.
94 E. Klimentova, J. Polacek, P. Simecek and P. Alexiou, *Front. Genet.*, 2020, **11**, 568546.
95 M. Barshai, A. Aubert and Y. Orenstein, *IEEE/ACM Trans. Comput. Biol. Bioinf.*, 2022, **19**, 1946–1955.
96 V. Rocher, M. Genais, E. Nassereddine and R. Mourad, *PLoS Comput. Biol.*, 2021, **17**, e1009308.
97 X. Shi, H. Teng and Z. Sun, *Briefings Bioinf.*, 2022, **23**, bbac441.
98 E. Y.-C. Chow, K. Lyu, C. K. Kwok and T.-F. Chan, *RNA Biol.*, 2020, **17**, 903–917.
99 E. Besnard, A. Babled, L. Lapasset, O. Milhavet, H. Parrinello, C. Dantec, J.-M. Marin and J.-M. Lemaitre, *Nat. Struct. Mol. Biol.*, 2012, **19**, 837–844.
100 S. Selvam, D. Koirala, Z. Yu and H. Mao, *J. Am. Chem. Soc.*, 2014, **136**, 13967–13970.
101 P. Shrestha, S. Jonchhe, T. Emura, K. Hidaka, M. Endo, H. Sugiyama and H. Mao, *Nat. Nanotechnol.*, 2017, **12**, 582–588.
102 V. González, K. Guo, L. Hurley and D. Sun, *J. Biol. Chem.*, 2009, **284**, 23622–23635.
103 K. Niu, L. Xiang, Y. Jin, Y. Peng, F. Wu, W. Tang, X. Zhang, H. Deng, H. Xiang, S. Li, J. Wang, Q. Song and Q. Feng, *Nucleic Acids Res.*, 2019, gkz484.
104 C.-Y. Lee, M. Joshi, A. Wang and S. Myong, *Nat. Commun.*, 2024, **15**, 3936.
105 S. Batra, B. Allwein, C. Kumar, S. Devbhandari, J.-G. Brüning, S. Bahng, C. M. Lee, K. J. Marians, R. K. Hite and D. Remus, *Science*, 2025, **387**, eadt1978.
106 A. Siddiqui-Jain, C. L. Grand, D. J. Bearss and L. H. Hurley, *Proc. Natl. Acad. Sci. U. S. A.*, 2002, **99**, 11593–11598.
107 M. Fry and L. A. Loeb, *J. Biol. Chem.*, 1999, **274**, 12797–12802.
108 S. D. Creacy, E. D. Routh, F. Iwamoto, Y. Nagamine, S. A. Akman and J. P. Vaughn, *J. Biol. Chem.*, 2008, **283**, 34626–34634.
109 D. Benhalevy, S. K. Gupta, C. H. Danan, S. Ghosal, H.-W. Sun, H. G. Kazemier, K. Paeschke, M. Hafner and S. A. Juranek, *Cell Rep.*, 2017, **18**, 2979–2990.
110 Z. Pietras, M. A. Wojcik, L. S. Borowski, M. Szewczyk, T. M. Kulinski, D. Cysewski, P. P. Stepien, A. Dziembowski and R. J. Szczesny, *Nat. Commun.*, 2018, **9**, 2558.
111 S. Ray, J. N. Bandaria, M. H. Qureshi, A. Yildiz and H. Balci, *Proc. Natl. Acad. Sci. U. S. A.*, 2014, **111**, 2990–2995.
112 H. Técher, S. Koundrioukoff, A. Nicolas and M. Debatisse, *Nat. Rev. Genet.*, 2017, **18**, 535–550.
113 I. Georgakopoulos-Soares, S. Morganella, N. Jain, M. Hemberg and S. Nik-Zainal, *Genome Res.*, 2018, **28**, 1264–1271.
114 T. Agarwal, S. Roy, S. Kumar, T. K. Chakraborty and S. Maiti, *Biochemistry*, 2014, **53**, 3711–3718.
115 S. Kumari, A. Bugaut, J. L. Huppert and S. Balasubramanian, *Nat. Chem. Biol.*, 2007, **3**, 218–221.
116 R. Shahid, A. Bugaut and S. Balasubramanian, *Biochemistry*, 2010, **49**, 8300–8306.
117 M. J. Gait, M. Komiyama, N. C. Seeman, O. Seitz, J. Micklefield and D. R. Liu, *Org. Biomol. Chem.*, 2012, **11**, 6537–6547.
118 P. Kumar, V. K. Yadav, A. Baral, P. Kumar, D. Saha and S. Chowdhury, *Nucleic Acids Res.*, 2011, **39**, 8005–8016.
119 R. K. Thakur, P. Kumar, K. Halder, A. Verma, A. Kar, J.-L. Parent, R. Basundra, A. Kumar and S. Chowdhury, *Nucleic Acids Res.*, 2009, **37**, 172–183.
120 L. Chen, J. Dickerhoff, K. Zheng, S. Erramilli, H. Feng, G. Wu, B. Onel, Y. Chen, K.-B. Wang, M. Carver, C. Lin, S. Sakai, J. Wan, C. Vinson, L. Hurley, A. A. Kossiakoff, N. Deng, Y. Bai, N. Noinaj and D. Yang, *Science*, 2025, **388**, eadr1752.
121 I. T. Holder and J. S. Hartig, *Chem. Biol.*, 2014, **21**, 1511–1521.
122 K. Paeschke, T. Simonsson, J. Postberg, D. Rhodes and H. J. Lipps, *Nat. Struct. Mol. Biol.*, 2005, **12**, 847–854.
123 P. Ruis and S. J. Boulton, *Genes Dev.*, 2021, **35**, 1–21.
124 J. S. Smith, Q. Chen, L. A. Yatsunyk, J. M. Nicoludis, M. S. Garcia, R. Kranaster, S. Balasubramanian, D. Monchaud, M.-P. Teulade-Fichou, L. Abramowitz, D. C. Schultz and F. B. Johnson, *Nat. Struct. Mol. Biol.*, 2011, **18**, 478–485.
125 M. Zhang, B. Wang, T. Li, R. Liu, Y. Xiao, X. Geng, G. Li, Q. Liu, C. M. Price, Y. Liu and F. Wang, *Nucleic Acids Res.*, 2019, **47**, 5243–5259.
126 J. W. Shay and W. E. Wright, *Nat. Rev. Genet.*, 2019, **20**, 299–309.
127 A. M. Zahler, J. R. Williamson, T. R. Cech and D. M. Prescott, *Nature*, 1991, **350**, 718–720.
128 A. L. Moye, K. C. Porter, S. B. Cohen, T. Phan, K. G. Zyner, N. Sasaki, G. O. Lovrecz, J. L. Beck and T. M. Bryan, *Nat. Commun.*, 2015, **6**, 7643.
129 M.-L. Zhang, X.-J. Tong, X.-H. Fu, B. O. Zhou, J. Wang, X.-H. Liao, Q.-J. Li, N. Shen, J. Ding and J.-Q. Zhou, *Nat. Struct. Mol. Biol.*, 2010, **17**, 202–209.
130 S. Neidle, *FEBS J.*, 2010, **277**, 1118–1125.
131 S. Neidle, *J. Med. Chem.*, 2016, **59**, 5987–6011.
132 S. Khateb, P. Weisman-Shomer, I. Hershco-Shani, A. L. Ludwig and M. Fry, *Nucleic Acids Res.*, 2007, **35**, 5775–5788.
133 S. Kumari, A. Bugaut and S. Balasubramanian, *Biochemistry*, 2008, **47**, 12664–12669.
134 M. M. Fay, P. J. Anderson and P. Ivanov, *Cell Rep.*, 2017, **21**, 3573–3584.

135 A. Khong, T. Matheny, S. Jain, S. F. Mitchell, J. R. Wheeler and R. Parker, *Mol. Cell*, 2017, **68**, 808–820.
136 J. L. Huppert, A. Bugaut, S. Kumari and S. Balasubramanian, *Nucleic Acids Res.*, 2008, **36**, 6260–6268.
137 T. Endoh, Y. Kawasaki and N. Sugimoto, *Angew. Chem., Int. Ed.*, 2013, **52**, 5522–5526.
138 E. G. Conlon, L. Lu, A. Sharma, T. Yamazaki, T. Tang, N. A. Shneider and J. L. Manley, *eLife*, 2016, **5**, e17820.
139 N. Maizels, *EMBO Rep.*, 2015, **16**, 910–922.
140 S.-R. Wang, Q.-Y. Zhang, J.-Q. Wang, X.-Y. Ge, Y.-Y. Song, Y.-F. Wang, X.-D. Li, B.-S. Fu, G.-H. Xu, B. Shu, P. Gong, B. Zhang, T. Tian and X. Zhou, *Cell Chem. Biol.*, 2016, **23**, 1113–1122.
141 Y. Wang, J. Wang, Z. Yan, J. Hou, L. Wan, Y. Yang, Y. Liu, J. Yi, P. Guo and D. Han, *Nucleic Acids Res.*, 2024, **52**, 2698–2710.
142 A. J. Hannan, *Nat. Rev. Genet.*, 2018, **19**, 286–298.
143 A. R. La Spada and J. P. Taylor, *Nat. Rev. Genet.*, 2010, **11**, 247–258.
144 S. M. Mirkin, *Nature*, 2007, **447**, 932–940.
145 Y. Wang, J. Wang, Z. Yan, J. Hou, L. Wan, Y. Yang, Y. Liu, J. Yi, P. Guo and D. Han, *Nucleic Acids Res.*, 2024, **52**, 2698–2710.
146 C. Zhao, G. Qin, J. Niu, Z. Wang, C. Wang, J. Ren and X. Qu, *Angew. Chem., Int. Ed.*, 2021, **60**, 432–438.
147 E. Ruggiero and S. N. Richter, *Nucleic Acids Res.*, 2018, **46**, 3270–3283.
148 A. Henderson, Y. Wu, Y. C. Huang, E. A. Chavez, J. Platt, F. B. Johnson, R. M. Brosh, D. Sen and P. M. Lansdorp, *Nucleic Acids Res.*, 2014, **42**, 860–869.
149 X.-C. Chen, G.-X. Tang, W.-H. Luo, W. Shao, J. Dai, S.-T. Zeng, Z.-S. Huang, S.-B. Chen and J.-H. Tan, *J. Am. Chem. Soc.*, 2021, **143**, 20779–20791.
150 S. Liu, L. Bu, Y. Zhang, J. Yan, L. Li, G. Li, Z. Song and J. Huang, *Anal. Chem.*, 2021, **93**, 5267–5276.
151 X.-B. Xu, Y.-Y. He, F. Wang, W. Chen, L. J. Tang and J.-H. Jiang, *Dyes Pigm.*, 2022, **201**, 110194.
152 T. Sakamoto, Z. Yu and Y. Otani, *Anal. Chem.*, 2022, **94**, 4269–4276.
153 J.-H. Yuan, J.-L. Tu, G.-C. Liu, X.-C. Chen, Z.-S. Huang, S.-B. Chen and J.-H. Tan, *Nucleic Acids Res.*, 2022, **50**, 4246–4257.
154 J.-N. Han, C. Zhong, M. Ge, S. Kuang and Z. Nie, *Chem. Sci.*, 2023, **14**, 4538–4548.
155 G. Lee, J. Park, S. H. Jang, S. Y. Lee, J. Seong, J. W. Jung, K. Kim, T. G. Hwang and J. Choi, *Molecules*, 2022, **27**, 2984.
156 Y. Liu, D. Zhang, Y. Qu, F. Tang, H. Wang, A. Ding and L. Li, *Chem. Biomed. Imaging*, 2024, **2**, 81–97.
157 S. Sasaki, G. P. C. Drummen and G. Konishi, *J. Mater. Chem. C*, 2016, **4**, 2731–2743.
158 W. Sun, M. Li, J. Fan and X. Peng, *Acc. Chem. Res.*, 2019, **52**, 2818–2831.
159 J. Zhang, H. Li, B. Lin, X. Luo, P. Yin, T. Yi, B. Xue, X.-L. Zhang, H. Zhu and Z. Nie, *J. Am. Chem. Soc.*, 2021, **143**, 19317–19329.
160 J. Berrones Reyes, P. S. Sherin, A. Sarkar, M. K. Kuimova and R. Vilar, *Angew. Chem., Int. Ed.*, 2023, **62**, e202310402.
161 X. Liu, D. Lin, Q. Wu, W. Yan, T. Luo, Z. Yang and J. Qu, *Acta Phys. Sin.*, 2018, **67**, 178701.
162 J. Robinson, S. G. Stenspil, K. Maleckaite, M. Bartlett, M. Di Antonio, R. Vilar and M. K. Kuimova, *J. Am. Chem. Soc.*, 2024, **146**, 1009–1018.
163 L. Liu, T. Ma, Y. Zeng, W. Liu, H. Zhang and Z. Mao, *Angew. Chem., Int. Ed.*, 2023, **62**, e202305645.
164 W. Liu, B.-C. Zhu, L.-Y. Liu, X.-Y. Xia, J. Jang, J. Dickerhoff, D. Yang and Z.-W. Mao, *Nucleic Acids Res.*, 2024, **52**, 9397–9406.
165 L. Liu, K. Wang, W. Liu, Y. Zeng, M. Hou, J. Yang and Z. Mao, *Angew. Chem., Int. Ed.*, 2021, **60**, 20833–20839.
166 T. R. Carver and C. P. Slichter, *Phys. Rev.*, 1953, **92**, 212–213.
167 F. Ni, *Prog. Nucl. Magn. Reson. Spectrosc.*, 1994, **26**, 517–606.
168 M. Mayer and B. Meyer, *Angew. Chem., Int. Ed.*, 1999, **38**, 1784–1788.
169 K. Zheng, S. Xiao, J. Liu, J. Zhang, Y. Hao and Z. Tan, *Nucleic Acids Res.*, 2013, **41**, 5533–5541.
170 Y. V. Suseela, N. Narayanaswamy, S. Pratihar and T. Govindaraju, *Chem. Soc. Rev.*, 2018, **47**, 1098–1131.
171 H. Huang, N. B. Suslov, N.-S. Li, S. A. Shelke, M. E. Evans, Y. Koldobskaya, P. A. Rice and J. A. Piccirilli, *Nat. Chem. Biol.*, 2014, **10**, 686–691.
172 Z.-H. Zhang, S. H. Qian, D. Wei and Z.-X. Chen, *Cell Biosci.*, 2023, **13**, 117.
173 A. Shivalingam, M. A. Izquierdo, A. L. Marois, A. Vyšniauskas, K. Suhling, M. K. Kuimova and R. Vilar, *Nat. Commun.*, 2015, **6**, 8178.
174 J. Mohanty, N. Barooah, V. Dhamodharan, S. Harikrishna, P. I. Pradeepkumar and A. C. Bhasikuttan, *J. Am. Chem. Soc.*, 2013, **135**, 367–376.
175 R.-X. Wang, Y. Ou, Y. Chen, T.-B. Ren, L. Yuan and X.-B. Zhang, *J. Am. Chem. Soc.*, 2024, **146**, 11669–11678.
176 Q. Li, J.-F. Xiang, Q.-F. Yang, H.-X. Sun, A.-J. Guan and Y.-L. Tang, *Nucleic Acids Res.*, 2013, **41**, D1115–D1123.
177 S. Xu, Q. Li, J. Xiang, Q. Yang, H. Sun, A. Guan, L. Wang, Y. Liu, L. Yu, Y. Shi, H. Chen and Y. Tang, *Nucleic Acids Res.*, 2015, gkv1040.
178 S. Xu, Q. Li, J. Xiang, Q. Yang, H. Sun, A. Guan, L. Wang, Y. Liu, L. Yu, Y. Shi, H. Chen and Y. Tang, *Sci. Rep.*, 2016, **6**, 24793.
179 S. Zhang, H. Sun, L. Wang, Y. Liu, H. Chen, Q. Li, A. Guan, M. Liu and Y. Tang, *Nucleic Acids Res.*, 2018, **46**, 7522–7532.
180 T.-Y. Wu, X.-C. Chen, G.-X. Tang, W. Shao, Z.-C. Li, S.-B. Chen, Z.-S. Huang and J.-H. Tan, *J. Med. Chem.*, 2023, **66**, 5484–5499.
181 J. Li, X. Yin, B. Li, X. Li, Y. Pan, J. Li and Y. Guo, *Anal. Chem.*, 2019, **91**, 5354–5361.
182 X. Tian, J. Li, Y. Zhang, Y. Gao, M. W. Afzal, A. Wang, T. D. James, Y. Bai and Y. Guo, *Sens. Actuators, B*, 2022, **359**, 131618.
183 A. Madireddy, P. Purushothaman, C. P. Loosbroock, E. S. Robertson, C. L. Schildkraut and S. C. Verma, *Nucleic Acids Res.*, 2016, **44**, 3675–3694.

184 M. Di Antonio, A. Ponjavic, A. Radzevičius, R. T. Ranasinghe, M. Catalano, X. Zhang, J. Shen, L.-M. Needham, S. F. Lee, D. Klenerman and S. Balasubramanian, *Nat. Chem.*, 2020, **12**, 832–837.
185 P. Kumar, A. Pandith, C.-L. Tseng and T. Burnouf, *J. Photochem. Photobiol., C*, 2023, **56**, 100619.
186 X. Teng, D. Hu, Y. Dai, H. Jing, W. Hu, Q. Zhang, N. Zhang and J. Li, *Angew. Chem., Int. Ed.*, 2024, **63**, e202407353.
187 M. Falabella, J. E. Kolesar, C. Wallace, D. De Jesus, L. Sun, Y. V. Taguchi, C. Wang, T. Wang, I. M. Xiang, J. K. Alder, R. Maheshan, W. Horne, J. Turek-Herman, P. J. Pagano, C. M. St. Croix, N. Sondheimer, L. A. Yatsunyk, F. B. Johnson and B. A. Kaufman, *Sci. Rep.*, 2019, **9**, 5605.
188 X. Wang, G. Qin, J. Yang, C. Zhao, J. Ren and X. Qu, *Nucleic Acids Res.*, 2024, gkae1259.
189 S. Takahashi, J. A. Brazier and N. Sugimoto, *Proc. Natl. Acad. Sci. U. S. A.*, 2017, **114**, 9605–9610.
190 K. T. McQuaid, S. Takahashi, L. Baumgaertner, D. J. Cardin, N. G. Paterson, J. P. Hall, N. Sugimoto and C. J. Cardin, *J. Am. Chem. Soc.*, 2022, **144**, 5956–5964.
191 V. S. Chambers, G. Marsico, J. M. Boutell, M. Di Antonio, G. P. Smith and S. Balasubramanian, *Nat. Biotechnol.*, 2015, **33**, 877–881.
192 G. Biffi, M. Di Antonio, D. Tannahill and S. Balasubramanian, *Nat. Chem.*, 2014, **6**, 75–80.
193 A. K. Todd, *Nucleic Acids Res.*, 2005, **33**, 2901–2907.
194 J. L. Huppert and S. Balasubramanian, *Nucleic Acids Res.*, 2007, **35**, 406–413.
195 Y. Yamaoki, A. Kiyoishi, M. Miyake, F. Kano, M. Murata, T. Nagata and M. Katahira, *Phys. Chem. Chem. Phys.*, 2018, **20**, 2982–2985.
196 S. Dzatko, M. Krafcikova, R. Hänsel-Hertsch, T. Fessl, R. Fiala, T. Loja, D. Krafcik, J. Mergny, S. Foldynova-Trantirkova and L. Trantirek, *Angew. Chem., Int. Ed.*, 2018, **57**, 2165–2169.
197 S. Manna, D. Sarkar and S. G. Srivatsan, *J. Am. Chem. Soc.*, 2018, **140**, 12622–12633.
198 S. Schoeftner and M. A. Blasco, *Nat. Cell Biol.*, 2008, **10**, 228–236.
199 H.-L. Bao and Y. Xu, *Chem. Commun.*, 2020, **56**, 6547–6550.
200 S. Karkare and D. Bhatnagar, *Appl. Microbiol. Biotechnol.*, 2006, **71**, 575–586.
201 P. E. Nielsen, M. Egholm, R. H. Berg and O. Buchardt, *Science*, 1991, **254**, 1497–1500.
202 G. L. Igloi, *Proc. Natl. Acad. Sci. U. S. A.*, 1998, **95**, 8562–8567.
203 S. K. Singh, A. A. Koshkin, J. Wengel and P. Nielsen, *Chem. Commun.*, 1998, 455–456.
204 B. Vester and J. Wengel, *Biochemistry*, 2004, **43**, 13233–13241.
205 M. A. Campbell and J. Wengel, *Chem. Soc. Rev.*, 2011, **40**, 5680.
206 M. Petersen, K. Bondensgaard, J. Wengel and J. P. Jacobsen, *J. Am. Chem. Soc.*, 2002, **124**, 5974–5982.
207 K. Zhang, Q. Nie, T. Chi-Kong Lau and C. Kit Kwok, *Angew. Chem., Int. Ed.*, 2024, **63**, e202310798.
208 L. Agnello, A. d'Argenio, R. Nilo, M. Fedele, S. Camorani and L. Cerchia, *Cancers*, 2023, **15**, 2010.
209 Y. Huang, G. Qin, T. Cui, C. Zhao, J. Ren and X. Qu, *Nat. Commun.*, 2023, **14**, 4647.
210 A. M. Chiarella, K. V. Butler, B. E. Gryder, D. Lu, T. A. Wang, X. Yu, S. Pomella, J. Khan, J. Jin and N. A. Hathaway, *Nat. Biotechnol.*, 2020, **38**, 50–55.
211 S. Konermann, M. D. Brigham, A. E. Trevino, J. Joung, O. O. Abudayyeh, C. Barcena, P. D. Hsu, N. Habib, J. S. Gootenberg, H. Nishimasu, O. Nureki and F. Zhang, *Nature*, 2015, **517**, 583–588.
212 X. Liu, S. Cui, Q. Qi, H. Lei, Y. Zhang, W. Shen, F. Fu, T. Tian and X. Zhou, *Nucleic Acids Res.*, 2022, **50**, 11387–11400.
213 G. Qin, Z. Liu, J. Yang, X. Liao, C. Zhao, J. Ren and X. Qu, *Nat. Cell Biol.*, 2024, **26**, 1212–1224.
214 L. Scipioni, A. Rossetta, G. Tedeschi and E. Gratton, *Nat. Methods*, 2021, **18**, 542–550.
215 Y. Kondo, H. Nonaka, Y. Takakusagi and S. Sando, *Angew. Chem., Int. Ed.*, 2021, **60**, 14779–14799.
216 R. Hänsel, S. Foldynová-Trantírková, F. Löhr, J. Buck, E. Bongartz, E. Bamberg, H. Schwalbe, V. Dötsch and L. Trantírek, *J. Am. Chem. Soc.*, 2009, **131**, 15761–15768.
217 X. Ren, J. Wei, X. Luo, Y. Liu, K. Li, Q. Zhang, X. Gao, S. Yan, X. Wu, X. Jiang, M. Liu, D. Cao, L. Wei, X. Zeng and J. Shi, *Advanced Science*, 2024, **11**, 2400829.
218 H. Lai, L. Wang, R. Qian, J. Huang, P. Zhou, G. Ye, F. Wu, F. Wu, X. Zeng and W. Liu, *Nat. Commun.*, 2024, **15**, 10223.
219 R. Hänsel-Hertsch, A. Simeone, A. Shea, W. W. I. Hui, K. G. Zyner, G. Marsico, O. M. Rueda, A. Bruna, A. Martin, X. Zhang, S. Adhikari, D. Tannahill, C. Caldas and S. Balasubramanian, *Nat. Genet.*, 2020, **52**, 878–883.
220 Y. Zhang, L. Wang, F. Wang, X. Chu and J.-H. Jiang, *J. Am. Chem. Soc.*, 2024, **146**, 15815–15824.
221 C. Li, G. Chen, Y. Zhang, F. Wu and Q. Wang, *J. Am. Chem. Soc.*, 2020, **142**, 14789–14804.
222 B. Chang, J. Chen, J. Bao, K. Dong, S. Chen and Z. Cheng, *Adv. Drug Delivery Rev.*, 2023, **192**, 114637.
223 P. Lesani, A. H. Mohamad Hadi, Z. Lu, S. Palomba, E. J. New and H. Zreiqat, *Commun. Mater.*, 2021, **2**, 108.
224 X. Ji, N. Wang, J. Wang, T. Wang, X. Huang and H. Hao, *Chem. Sci.*, 2024, **15**, 3800–3830.
225 X. Jiang, L. Wang, S. L. Carroll, J. Chen, M. C. Wang and J. Wang, *Antioxid. Redox Signaling*, 2018, **29**, 518–540.
226 C. Liu, H. Ma, Z. Hu, R. Tian, R. Ma, Y. Xu, X. Wang, X. Zhu, P. Yu, S. Zhu, H. Sun and Y. Liang, *Front. Chem.*, 2019, **9**, 739802.
227 M. L. Metzker, J. Lu and R. A. Gibbs, *Science*, 1996, **271**, 1420–1422.
228 A. Loudet and K. Burgess, *Chem. Rev.*, 2007, **107**, 4891–4932.
229 Z. Shi, X. Han, W. Hu, H. Bai, B. Peng, L. Ji, Q. Fan, L. Li and W. Huang, *Chem. Soc. Rev.*, 2020, **49**, 7533–7567.
230 H. Cheng, X. Cao, S. Zhang, K. Zhang, Y. Cheng, J. Wang, J. Zhao, L. Zhou, X. Liang and J. Yoon, *Adv. Mater.*, 2023, **35**, 2207546.
231 S. Zeng, X. Liu, Y. S. Kafuti, H. Kim, J. Wang, X. Peng, H. Li and J. Yoon, *Chem. Soc. Rev.*, 2023, **52**, 5607–5651.
232 L. Wang, W. Du, Z. Hu, K. Uvdal, L. Li and W. Huang, *Angew. Chem., Int. Ed.*, 2019, **58**, 14026–14043.

233 X. Chen, T. Pradhan, F. Wang, J. S. Kim and J. Yoon, *Chem. Rev.*, 2012, **112**, 1910–1956.
234 M. Le Fur, N. J. Rotile, C. Correcher, V. Clavijo Jordan, A. W. Ross, C. Catana and P. Caravan, *Angew. Chem., Int. Ed.*, 2020, **59**, 1474–1478.
235 J. Wahsner, P. Désogère, E. Abston, K. A. Graham-O'Regan, J. Wang, N. J. Rotile, M. D. Schirmer, D. D. Santos Ferreira, J. Sui, B. C. Fuchs, M. Lanuti and P. Caravan, *J. Am. Chem. Soc.*, 2019, **141**, 5593–5596.
236 R. Lo, A. Majid, G. O. Fruhwirth and R. Vilar, *Bioorg. Med. Chem.*, 2022, **76**, 117097.